Measurements of OH and RO$_2$ radicals at Dome C, East Antarctica

A. Kukui[1,4], M. Legrand[2], S. Preunkert[2], M. M. Frey[3], R. Loisil[5], J. Gil Roca[1], B. Jourdain[2], M. D. King[6], J. L. France[6] and G. Ancellet[1]

[1]{LATMOS, CNRS, Paris, France}

[2]{LGGE, CNRS, Grenoble, France}

[3]{BAS, NERC, Cambridge, UK}

[4]{LPC2E, CNRS, Orléans, France}

[5]{ Division Technique, INSU, Meudon, France}

[6] {Department of Earth Sciences, Royal Holloway University of London, Egham, Surrey, UK, TW20 OEX}

Correspondence to: A. Kukui (alexandre.kukui@cnrs-orleans.fr)

Abstract

Concentrations of OH radicals and the sum of peroxy radicals, RO$_2$, were measured in the boundary layer for the first time on the East Antarctic Plateau at the Concordia Station (Dome C, 75.10° S, 123.31° E) during the austral summer 2011/2012. The median concentrations of OH and RO$_2$ radicals were 3.1×10^6 molecule cm^{-3} and 9.9×10^7 molecule cm^{-3}, respectively. These values are comparable to those observed at the South Pole, confirming that the elevated oxidative capacity of the Antarctic atmospheric boundary layer found at the South Pole is not restricted to the South Pole but common over the high Antarctic plateau. At Concordia, the concentration of radicals showed distinct diurnal profiles with the median maximum of 5.2×10^6 molecule cm^{-3} at 11:00 and the median minimum of 1.1×10^6 molecule cm^{-3} at 1:00 for OH radicals and 1.7×10^8 molecule cm^{-3} and 2.5×10^7 molecule cm^{-3} for RO$_2$ radicals at 13:00 and 23:00, respectively (all times are local times). Concurrent measurements of O$_3$, HONO, NO, NO$_2$, HCHO and H$_2$O$_2$ demonstrated that the major primary source of OH and RO$_2$ radicals at Dome C was the photolysis of HONO, HCHO and

1   H_2O_2, with the photolysis of HONO contributing ~75% of total primary radical production.

2   However, photochemical modelling with accounting for all these radical sources

3   overestimates the concentrations of OH and RO_2 radicals by a factor of 2 compared to field

4   observations. Neglecting the net OH production from HONO in the photochemical modelling

5   results in an underestimation of the concentrations of OH and RO_2 radicals by a factor of 2.

6   To explain the observations of radicals in this case an additional source of OH equivalent to

7   about (25-35)% of measured photolysis of HONO is required. Even with a factor of 5

8   reduction in the concentrations of HONO, the photolysis of HONO represents the major

9   primary radical source at Dome C. To account for a possibility of an overestimation of NO_2

10   observed at Dome C the calculations were also performed with NO_2 concentrations estimated

11   by assuming steady state NO_2/NO ratios. In this case the net radical production from the

12   photolysis of HONO should be reduced by a factor of 5 or completely removed based on the

13   photochemical budget of OH or 0D modelling, respectively. Another major factor leading to

14   the large concentration of OH radicals measured at Dome C was large concentrations of NO

15   molecules and fast recycling of peroxy radicals to OH radicals.

16

17 **1. Introduction**

18   Atmospheric chemistry in polar regions has gained growing interest over the two last

19   decades due to the discovery of surprisingly high photochemical activity in both Antarctic and

20   Arctic, i.e. at the South Pole (Mauldin et al., 2001; Davis et al., 2001) and at Summit,

21   Greenland (Honrath et al., 1999; Sjostedt et al., 2007). The photochemistry of the boundary

22   layer atmosphere (BL) at these snow covered regions is significantly influenced by the

23   emissions of reactive gases from the snowpack. The emissions are produced by the interaction

24   of solar radiation and photo-chemically active species in the snowpack (e.g. Grannas et al.,

25   2007 for a review).

26   At the South Pole (SP) unexpectedly large concentrations of OH radicals in the

27   boundary layer, about 2×10^6 molecule cm^{-3}, were observed for the first time during ISCAT

28   1998 (Mauldin et al., 2001) and were confirmed in later campaigns (ISCAT 2000 (Mauldin et

29   al., 2004), ANTCI 2003 (Mauldin et al., 2010)). The elevated concentrations of OH radicals

30   were explained by fast recycling of OH radicals from peroxy radicals in presence of large

31   concentrations of NO. The large concentration of NO molecules exceeded free tropospheric

32   concentrations (Davis et al., 2001) and was attributed to the release of NO_x from snowpack

1 (following UV photolysis of the nitrate anion (NO_3^-) on/in snow grains (Jones et al., 2001))

2 and its accumulation in a stable and shallow BL at the SP (Davis et al., 2001, 2004, 2008).

3 The build up of large concentrations of NO_x at the SP was suggested to be enhanced by the

4 continuous sunlight during summer and the location at the bottom of a large air drainage

5 basin. (Davis et al., 2004, 2008).

6 At the SP the major gas-phase net sources of OH and HO_2 radicals were found to be the

7 photolysis of HCHO and H_2O_2. The production of OH radical from O_3 photolysis was found

8 to be less important owing to the small concentration of water at such low temperatures. The

9 photochemical box model for the SP tends to slightly overpredict the concentrations of OH

10 compared to observations, although satisfactorily reproduces the dependence of the

11 concentration of OH on the concentration of NO (Chen et al., 2004; Mauldin et al., 2004). It

12 has to be emphasized that when considering the mixing ratio of ~30 pptv of HONO measured

13 at the SP by using mist chamber/Ion Chromatography method (Dibb et al., 2004) the model

14 overpredicts concentrations of OH radicals at the SP by a factor of 3 to 5 (Chen et al., 2004).

15 It was proposed that the HONO concentrations derived with the mist chamber/Ion

16 Chromatography method during these campaigns were probably biased by some systematic

17 error (e.g., chemical interference) (Chen et al., 2004).

18 Conditions favouring the accumulation of large concentrations of NO_x were thought to

19 be specific to the South Pole (24 h sunlight and shallow stable boundary layer), however a

20 larger part of Antarctic Plateau also experiences elevated concentrations of NO_x despite

21 strongly reduced solar radiation at night and the resulting build up of an unstable convective

22 atmospheric boundary layer. This is supported by airborne observations of large

23 concentrations of NO (Davis et al., 2008; Slusher et al., 2010, Wang et al., 2007) showing that

24 a shallow photochemicaly active layer is common for large part of Antarctic Plateau

25 atmosphere. However, these airborne measurements of NO_x remain limited in time and space.

26 In addition, although the elevated concentrations of NO_x represent the key factor in build up

27 of large OH concentrations in the polar BL, the relationship of concentrations of OH with

28 concentrations of NO is nonlinear (Mauldin et al., 2004). Thus, an accurate prediction of the

29 concentration of OH radical in other Antarctic regions may be difficult without detailed

30 information on the radical primary production and net losses. These uncertainties in part

31 motivated the OPALE (Oxidant Production in Antarctic Lands and Export) project aiming at

1 a characterisation of the oxidative capacity of the BL atmosphere in the region of East
2 Antarctica.

3   In addition to the monitoring of surface ozone, that was initiated in 2007 at the
4 Concordia station on the East Antarctic plateau (Legrand et al., 2009), two others studies
5 related to the BL photochemistry have been performed at that site prior to the OPALE
6 campaign: The measurements of gas-phase NO concentrations and for the first time on the
7 Antarctic plateau measurements of gas-phase NO_2 concentrations were conducted during
8 summer 2009/2010 by Frey et al. (2013). Frey et al. (2013) revealed that concentrations of
9 NO at Dome C are comparable to those observed at the SP but the ratios $[NO_2]/[NO]$ were
10 found to be significantly larger than calculated assuming photostationary state conditions with
11 measured concentrations of O_3 and NO. As a possible explanation Frey et al. (2013)
12 suggested significantly larger peroxy radical concentrations at Dome C than at the SP. The
13 study of Frey et al., (2013) also revealed a distinct diurnal cycle of NO_x that has been
14 attributed to boundary layer stability and the flux of NO_x released from the snowpack both
15 driven by diel changes in solar radiation (France et al., 2011). The second study was dedicated
16 to the measurements of concentrations of HONO during the summer 2010/2011 (Kerbrat et
17 al., 2012) with a LOPAP technique. Kerbrat et al. (2012) concluded that the observed large
18 mixing ratio (~30 pptv) of HONO would require an unexpectedly large photochemical source
19 of HONO from the snowpack, if the measurements of gas-phase HONO were not biased due
20 to an unknown interference.

21   In the framework of the OPALE project aimed at characterisation of the oxidative
22 capacity of the atmosphere in the region of East Antarctica (Preunkert el al., 2012) a field
23 campaign was carried out at the top of the high Antarctic Plateau, at Concordia station, from
24 December 2011 to January 2012. The first results of this campaign are presented in several
25 publications accompanying this article, including (Frey et al., this issue) for NO and NO_2,
26 (Legrand et al., this issue) for HONO, and (Preunkert et al., this issue) for HCHO. Here
27 presented for the first time are measurements of concentrations of OH and RO_2 radicals
28 conducted on the East Antarctic Plateau at the Concordia station (Dome C). Sources and sinks
29 of these radicals are discussed in the light of concurrent chemical observations made during
30 the campaign, including HONO, NO, NO_2, H_2O_2, HCHO, and O_3, as well as surface
31 meteorological parameters, physics of the boundary layer and photolysis rates.

32

2. Methods

Measurements of atmospheric concentration of OH and RO_2 (the sum of hydroperoxy HO_2 and organic peroxy radicals) radicals were conducted from 19 December 2011 to 9 January 2012 at Concordia station (Dome C, 75.10° S, 123.31° E, altitude 3233 m).

The weather at Concordia is dominated by weak katabatic winds (~3 m s^{-1}) and clear sky conditions with frequent presence of elevated cirrus clouds. Daylight lasts 24 h with a significant diurnal variation of solar radiation (as shown in Figures 1a and 1b for the photolysis rate coefficients for NO_2 and O_3) resulting in a strong diurnal cycle in near-surface temperature (Figure 1c) and wind speed. During the OPALE campaign the median values of the temperature at height of 1m and the wind speed ranged from -36°C and 2 m s^{-1} at 03:00 (all times are local times equivalent to UTC+8 h.) to -27°C and 4 m s^{-1} at 15:00, respectively. The diurnal solar cycle is responsible for a well defined diurnal cycle of boundary layer structure (Figure 1c). Starting from about 7:00 in the morning the diurnal heating and upward sensible heat flux (King et al., 2006) drive formation of the convective mixing layer reaching a maximum height of 300-600 m at about 17:00. During the night the boundary layer is stably stratified and confined to a height of several meters. The boundary layer height presented in Figure 1c comes from the Modèle Atmosphérique Régional (MAR) (Gallée et al., this issue) briefly described in Section 2.3.

The measurement site was located in a designated clean-air sector 0.7 km to the south of the main station buildings. During the measurement period the wind direction was predominantly from the south, median value of 180°, with few pollution events (on 19-Dec, 31-Dec and 1-Jan) due to the wind coming from the station, wind sector of 10 - 50° (Figure 1c). The data corresponding to the pollution events were filtered out.

2.1 Radical measurements

Concentrations of OH and RO_2 radicals, as well as sulfuric acid (not shown here), were measured using chemical ionisation mass spectrometry (CIMS) (Eisele and Tanner, 1991; Berresheim et al., 2000). Detailed description of the instrument is presented elsewhere (Kukui et al., 2008; Kukui et al., 2012; Michoud et al., 2012). Here we briefly present the principle of the method and report details about the setup of the device and working conditions applied during measurements at Dome C.

1   The concentration of OH radical was measured by titrating atmospherically sampled

2   OH radicals with SO_2 to form H_2SO_4 in a chemical conversion reactor in the presence of

3   water vapor and oxygen [Eisele and Tanner, 1991; Tanner et al., 1997; Berresheim et al.,

4   2000]. H_2SO_4 was detected by mass spectrometry as the HSO_4^- ion. The HSO_4^- ion was

5   produced by chemical ionisation with NO_3^- in an ion-molecule reactor following the

6   chemical conversion reactor. To distinguish for atmospheric sulfuric acid the chemical

7   titration was performed using isotopically labelled $^{34}SO_2$ leading to the formation of $H_2^{34}SO_4$.

8   The concentration of total peroxy radicals RO_2 was measured by converting RO_2 into OH

9   radicals via reactions with NO injected in the chemical conversion reactor [Reiner et al.,

10   1997] followed by conversion of OH into sulfuric acid.

11   During measurements at Dome C and similarly to previous measurements in Coastal

12   Antarctica at Dumont d'Urville (DDU) (Kukui et al., 2012) the instrument was installed in a

13   shipping container with the chemical conversion reactor fixed to the roof of the container via

14   an interface cap covered with a PTFE sheet. The sampling aperture of the reactor (3 mm

15   diameter) was positioned 50 cm above the roof and about 3 m above the snow surface.

16   Ambient air was sampled at a volumetric flow rate of 7.4 standard litres (sl) min^{-1}

17   creating turbulent flow in the chemical conversion region of the reactor (Reynolds Number

18   $Re = 6400$). The turbulent flow conditions minimize possible influence of wind speed on the

19   measurements and ensure fast mixing of reactants. The reactants used for the chemical

20   conversion ($^{34}SO_2$ and NO) and the radical quencher (NO_2) are introduced into the reactor

21   through a set of injectors. NO_2 used as a scavenger removes not only the OH radicals, but also

22   peroxy radicals converting them into HO_2NO_2 and RO_2NO_2 nitrates. The input flow rates of

23   the reactants were similar to those previously used with this instrument (e.g. Kukui et al.,

24   2012), while the sampling flow rate was a factor of 2 smaller than usual. These flow rates

25   were necessary to compensate for the reduced pressure at Dome C (620 hPa) compared to sea-

26   level operation of the instrument, and provided comparable reaction times to previous

27   deployments of this instrument. Switching the reactant flows between the different injectors

28   allows measurements in four different modes: the background mode, two different OH radical

29   measurement modes and the RO_2 radical measurement mode. The two OH measurement

30   modes differ by the time used for the chemical conversion, 4 and 20 ms (Kukui et al., 2008;

31   Kukui et al., 2012). Ratio of the signals with the short and the long conversion times may be

32   used as an indicator of an artificial OH formation in the reactor [Kukui et al., 2008].

Measurements of OH, RO_2 and H_2SO_4 were performed by monitoring the peak intensities at m/z=62 (NO_3^-), m/z=99 ($H^{34}SO_4^-$) and m/z=97 ($H^{32}SO_4^-$). The detection of $H^{34}SO_4^-$ and $H^{32}SO_4^-$ corresponds to the measurement of the radicals (OH or RO_2) and H_2SO_4, respectively. The ion peak intensities were measured sequentially resulting in nine measurements of OH and one measurement of RO_2 for every 28 minutes. Every measurement of OH was derived from 1 min of OH ion signal count and two 30 s background ion signal counts before and after the OH signal measurement. RO_2 was measured at the end of the OH detection sequence by switching on the NO flow to the corresponding injector for the duration of 2 min. To avoid any possible influence of traces of NO on the OH measurements a time delay of 10 min was introduced after switching off the NO flow and before starting the next OH measurement sequence to ensure flushing of the chemical conversion reactor. The measurements of OH and RO_2 radicals were averaged to 15 minute and 30 minute time intervals, respectively.

The concentration of the radicals, [R], is derived from the measured ratio of the $H^{34}SO_4^-$ and NO_3^- ion peak intensities, I_{99}/I_{62}: $[R] = C_R \times \ln (1 + I_{99} / I_{62})$, where C_R is a calibration coefficient determined in calibration measurements by production of a known concentration of OH or RO_2 radicals in a turbulent flow reactor by photolysis of water vapor at 184.9 nm (Heard and Pilling, 2003, and references therein; Faloona et al., 2004; Dusanter et al., 2008). Except for additional thermo-stabilisation of a Pen-Ray mercury lamp and a VUV phototube the construction of the calibration cell was the same as previously described in Kukui et al., (2008). The concentration of OH and HO_2 radicals generated in the turbulent flow was calculated from the monitored photon flux and H_2O concentration. For precise control of the concentrations of H_2O at low temperatures the gas manipulation system for the introduction of the mixture of pure air and water vapor into the photolysis reactor was modified by replacing the previously used water trap by a liquid flow controller (Bronkhorst, μ-FLOW series L01, 1.4 g/h) allowing simulation of typical atmospheric humidities encountered at Dome C (e.g., 50-70% at -30°C). During the calibrations at Dome C the previously employed cooled mirror dew-point transmitter used for the humidity measurements in the photolysis reactor was found to be unreliable at low temperatures and was replaced by a capacitive humidity sensor (Vaisala, HMP155) providing more accurate humidity data. The water vapor/air mixture was generated inside the container and introduced to the calibration cell positioned on the roof of the container through a 10m Teflon tube placed outside of the container, providing the cooling of the calibration gas mixture to the

1 ambient temperature. Despite these modifications frequent difficulties were encountered

2 maintaining stable humidity under conditions of low temperatures at Dome C, limiting

3 calibration accuracy.

4 The atmospheric concentration of total peroxy radicals RO_2 was measured assuming

5 that the HO_2 and CH_3O_2 radicals represent the major part of all RO_2 radicals at Dome C, i.e.

6 $[RO_2] = [HO_2] + [CH_3O_2]$, with a ratio of $[HO_2]/[RO_2]$ of about 0.7, as informed from the

7 model calculations (see below). The calibration of HO_2 and CH_3O_2 was performed by adding

8 into the calibration cell photolysis reactor either CO or CH_4 converting any OH radical to

9 HO_2 or CH_3O_2, respectively [Hanke et al., 2002; Fuchs et al., 2008]. The sensitivity to HO_2

10 was found to be (15±2)% higher than that for the CH_3O_2.

11 The overall accuracy of the calibration coefficients was estimated taking into account

12 uncertainties of all parameters used for calculation of the radical concentrations in the

13 photolysis reactor and the precision of the measurements of the ratio I_{99}/I_{62}. The main sources

14 of the calibration uncertainty at Dome C were the estimation of the photon flux (±15%) and

15 the uncertainty of the measurement of humidity (±30%). The overall estimated calibration

16 accuracy (2σ) was of 36% for OH and of 40% for HO_2. The uncertainty of the measurements

17 of RO_2, accounting for possible variation of the RO_2 composition, was estimated to be of 45%

18 at Dome C. Accounting for the calibration uncertainties and measurement precision, the

19 overall 2σ uncertainty of the 15 min averaged measurements of OH and RO_2 was estimated to

20 be 40% and 47% during the day time and 60% and 50% during the night time, respectively.

21 The lower limits of detection for OH and RO_2 radicals at signal-to-noise ratio of 3 and a 2

22 minute integration time were 5×10^5 molecule cm^{-3} and 2×10^6 molecule cm^{-3}, respectively.

23 To avoid possible contamination of ambient air by the SO_2, NO and NO_2 reactants

24 added to the chemical conversion reactor, a trap was set up at the pumps exhaust by using two

25 100 L cylinders containing zeolites. The cylinders were refilled several times during

26 measurements. Flexible exhaust tube of 30 m length was always placed downwind from the

27 container. When the exhaust tube was intentionally placed upwind and close to the radicals

28 sampling point no effect on radical measurements was detected. Also, no influence of the

29 exhaust on the measurements of NO_x and HONO could be noticed.

2.2 Other measurements

Other chemical measurements conducted at Dome C during the campaign that are relevant to the discussion of sources and sinks of OH and RO_2 radicals include O_3, HCHO, H_2O_2, HONO, NO, NO_2 and photolysis coefficient values. Their mean values and ranges are summarised in Table 1, while the detailed discussion of these data and description of the instruments and applied working conditions during the campaign are presented in the corresponding companion papers.

Surface ozone was monitored by UV absorption (Thermo electron Corporation model 49I) deployed at Dome C since 2007 (Legrand et al., 2009). Atmospheric HCHO measurements were performed with a fluorimetric method using commercial Aerolaser analyzer (model AL-4021) (Preunkert et al., 2014, and this issue). A fluorimetric two-channel technique was applied for determinations of H_2O_2 (Aerolaser, Model AL2021)(Preunkert et al., 2012).

NO_x was measured with a 2-channel chemiluminescence detector with one channel used for NO detection and the other for the sum of NO and NO originating from the quantitative photolytic conversion of NO_2 (Bauguitte et al., 2012; Frey et al., 2013, and this issue). The NO_2 and NO measurements are discussed in Frey et al. (this issue). The ratios of NO_2 to NO observed at Dome C during 2011-2012 campaign were up to 3 times larger than in 2009-2010 (Frey et al., 2013) and significantly larger, up to 7 times, than the ratios estimated assuming photochemical steady-state (PSS) conditions for NOx. It is suggested that some part of this inconsistency may be due to unknown interference leading to an overestimation of the NO_2 concentrations (Frey et al., this issue).

The photolysis rate constants, J, were calculated from measurements of "actinic flux" (Madronich 1987) measured by a Met-Con 2π spectral radiometer with a CCD detector and a spectral range from 285 to 700 nm. The Met-Con Spectral radiometer was calibrated before and after the campaign using a NIST traceable standard 1000 W tungsten halogen lamp. No significant changes were observed in the performance of the spectral radiometer. The spectral radiometer was mounted on a mast of 1m height on the roof of the container used for the radical measurements. A shadow band was fitted to provide a horizontal horizon. Downwelling unweighted radiance over a complete hemisphere, was recorded as a 5 second average for each of the 532 pixels and internally interpolated to a 1nm resolution over 285-700 nm. The atmospheric photolysis coefficients, J, were calculated using the measured

actinic flux along with quantum yields and absorption cross-sections from Sander et al., (2011). The principle of using a 2π CCD Met-Con spectral radiometer to accurately determine photodissociation rate constants, J, has been previously demonstrated by Jäkel et al., (2007). Total 4π steradian radiance was calculated by multiplying the downwelling 2π steradian radiance by a value of 1.9. The value of 1.9 is based on measurements of downwelling and upwelling radiance by inverting the spectral radiometer.

HONO was measured with a long path absorption photometry (LOPAP) ((Heland et al., 2001; Kleffmann et al., 2002) at height of 1m above the snow surface. In spite of the use of the LOPAP, thought to be free of measurement artefacts, mixing ratios of HONO observed at Dome C in December 2011/January 2012 (hourly means of 35 ± 5 pptv, Legrand et al., this issue) are in the same range as previously observed in December 2010/January 2011 (hourly means of 30.4 ± 3.5 pptv) by Kerbrat et al. (2012). As discussed by Legrand et al. (this issue), laboratory experiments with irradiated surface snows collected at Concordia reveal that the snowpack may be a very significant source of HONO. It is shown that this source only accounts for a third of the observed HONO mixing ratios at 1 m height at Concordia. Legrand et al. (this issue) report tests done both in the field and in the lab that tend to suggest an overestimation of HONO measurements in the range of 10 to 20 pptv due to the presence of HO_2NO_2 in the range of 50-100 pptv in the cold atmosphere at Dome C.. This range of HO_2NO_2 mixing ratios is in agreement with the median $[HO_2NO_2]$ of 80 pptv estimated from RO_2 and NO_2 levels measured at Dome C (see Section 3.2). Also, as discussed by Legrand et al. (this issue), similar levels of HO_2NO_2 were previously observed in Antarctica.

2.3 Model calculations

Observed concentrations of OH and RO_2 were compared with those calculated using a 0D box model. Photostationary concentrations of OH and RO_2 were calculated by performing numerical integration using a subset from the Master Chemical Mechanism, MCM v3.2 (Jenkin et al., 1997; Saunders et al., 2003) (website: http://mcm.leeds.ac.uk/MCM). The subset includes 159 reactions comprising the MCM inorganic section, photochemistry, loss of HNO_3 and RO_2NO_2 by dry deposition and methane chemistry extended with CH_3CHO and CH_3COCH_3. The model ran using the MATLAB package for the entire period from 19th December to 10th January with 15 min time step and initiated by three-day spin-up for the first day. The calculations were constrained by the 15 min averaged measurements of HONO, NO, NO_2, O_3, HCHO, H_2O_2, photolysis coefficients and meteorological parameters. Concentration

1   levels of CO, CH$_4$, H$_2$, CH$_3$CHO, CH$_3$OOH, CH$_3$COCH$_3$ and CH$_3$COOH, were estimated as

2   described in Section 3.2.

3   The vertical distribution of HONO in the boundary layer was modelled using a 1D

4   chemistry-transport box model with a vertical distribution of turbulent diffusivity and

5   boundary layer heights calculated by the regional atmospheric MAR model (Modèle

6   Atmosphérique Régional). A detailed description of the model and its validation with respect

7   to observations from the Automatic Weather Station at Dome C is given in Gallée and

8   Gorodetskaya (2008), Gallée et al., (this issue) and references therein. The turbulence scheme

9   is based on an E-e scheme and on the Monin-Obukhov Similarity theory (MOST), outside and

10   inside the lowest model layer of MAR, respectively. Similar to calculations performed by

11   Legrand et al., (this issue), we used the MAR data obtained with a horizontal resolution of 20

12   km centred at Dome C; a vertical resolution of 0.9 m up to a height of 23 m above the surface

13   increasing upward to about 50 m at the height of 500 m; 100 vertical levels with a top level at

14   1 hPa. For the 1D box model calculations the values of the vertical diffusivity, Kz, were

15   linearly interpolated to the vertical grid of 0.1 m from the surface to 5 m, 0.2 m from 5 to 7 m,

16   0.5 m from 7 to 10 m, around 1 m from 10 to 20 m and then increases up to 120 m at 1200 m

17   height (the BL upper bound was always lower than 1200 m during the OPALE campaign).

18   The boundary layer height is defined by MAR as the height where the turbulent kinetic

19   energy decreases below 5 % of the value at the lowest layer of the model. The calculated

20   boundary layer height profile, as well as measured temperature and wind direction profiles are

21   presented in Figure 1.

22

23   **3.   Results and Discussion**

24   **3.1   Presentation of the measurements of OH and RO$_2$ radicals**

25   Measurements of the concentration of OH and RO$_2$ radicals are presented in Figures 1

26   and 2. The radical concentrations exhibited clear diurnal profiles driven by the solar radiation

27   cycle and ranged from 3×10^5 to 7.5×10^6 and from 1×10^7 to 2×10^8 for OH and RO$_2$,

28   respectively, in units of molecule cm^{-3}. As shown in Figure 2, the diurnal profiles of OH and

29   RO$_2$ radicals follow the diurnal variation of the NO$_2$ photolysis coefficient, J(NO$_2$). At the

30   same time, one can notice some deviation of the diurnal concentration profiles of OH and RO$_2$

31   from the J(NO$_2$) profile with larger concentrations for OH and lower for RO$_2$ in the afternoon.

This is reflected in the diurnal profile of the ratio of [OH] to [RO$_2$] (Figure 2c) which shows a diurnal profile with lower values of [OH]/[RO$_2$] during the day and factor of ~2 larger in the afternoon. Notably, the [OH]/[RO$_2$] diurnal profile correlates with the daily profile of the concentration of NO (Figure 2c).

The median concentrations of RO$_2$ and OH radicals measured at Dome C are compared to those observed at the South Pole in Table 1. At Dome C the J(O(^{1}D)) daily median values at 5:00 and 19:00 (9×10^{-6} s^{-1}) are similar to median J(O(^{1}D)) observed at the SP ((8.5-9.0)×10^{-6} s^{-1}). Comparing the corresponding concentrations of OH radical one can see that the median values at Dome C are close to that observed at the SP for 5:00 and somewhat higher at 19:00, 2.5×10^6 and 3.8×10^6, respectively, compared to 2.3×10^6 at the SP during ISCAT 2000. The concentrations of NO at the SP were similar to the observed at Dome C, 88 pptv and 77 pptv, respectively.

As seen in Figure 3, the concentrations of both OH and RO$_2$ correlate linearly with J(NO$_2$) with about 60% and 80% of the variability of OH and RO$_2$, respectively, explained by the variability of J(NO$_2$). The relationship of [OH] with J(O(^{1}D)), although with a large scattering as in the case with J(NO$_2$), was close to a power-law dependence with an exponent of ~0.5 in accordance with a typical close to quadratic dependence of J(O(^{1}D)) on J(NO$_2$) observed at Dome C. As seen from the color coding in Figure 3 by concentration of NO of the graph points, there is an obvious correlation with [NO], positive for [OH] and negative for [RO$_2$]. In fact, about 80% of the [OH]/[RO$_2$] variability may be explained by the linear correlation with [NO] (Figure 3c).

The important role of NO in controlling the concentrations of OH and RO$_2$ is seen on Figure 4 where [OH] and [RO$_2$] are normalised by J(NO$_2$) to remove the dependence on solar radiation and plotted against [NO]. For concentrations of NO of up to ~150 pptv the concentration of OH rises and then levels off, while [RO$_2$] exhibits the reverse dependence on [NO]. These dependences are very similar to those observed at the SP (Figures 2 and 7 in Mauldin et al., 2004) and can be explained in a similar way: when the concentration of NO is small, the concentration of OH increases due to the enhanced recycling from RO$_2$ until the losses of RO$_2$ and OH in reactions with NO$_2$ become important compared to other loss processes and therefore compensate the enhanced OH formation (see below for further discussion).

1   Owing to an approximate linear correlation of [HONO] with [NO] observed at Dome C

2   (Legrand et al., this issue) together with a approximately linear relation between J(HONO)

3   and J(NO$_2$) the dependence of the concentrations of OH and RO$_2$ on J(HONO) and HONO is

4   very similar to that on J(NO$_2$) and [NO] presented in Figures 3 and 4, implying the

5   concentration of HONO also could be an important parameter controlling the radical

6   variability.

7   ## 3.2   Radical sources and sinks

8   The sources and sinks of OH and RO$_2$ radicals at Dome C were calculated using the

9   radical field measurements and other available relevant observations presented in Table 1.

10   Some of the key species involved in the radical production and losses, namely CO, CH$_4$ and

11   H$_2$, were not measured. For CO, a mixing ratio of 40 ± 4 ppbv was assumed referring to the

12   value observed at the South Pole (Novelli and Masarie, 2013). Similar mixing ratios of CO

13   for the period of December - January have been measured during ISCAT 2000 at the SP

14   (Davis et al., 2004), at DDU (Preunkert et al., 2012). For methane and H$_2$ mixing ratios the

15   values of 1.8 ppmv ((Steele et al., 2002) and 520 ppbv (Steele et al., 2003) are adopted,

16   respectively, based on measurements made at other Antarctic sites.

17   Measurements of acetaldehyde are sparse in Antarctic regions. As discussed by

18   Legrand et al. (2012), at the coastal site of DDU an acetaldehyde background mixing ratio

19   close to 80 pptv can be assumed, though this value may be highly variable over the Southern

20   ocean (5 to 50 pptv). Hamer et al., (2007) reported a mixing ratio of CH$_3$CHO of 60 pptv at

21   the SP. In our calculations we used a value of 60 pptv with an uncertainty of 20%. Methyl

22   hydroperoxide (CH$_3$OOH), acetic acid (CH$_3$COOH) and acetone (CH$_3$COCH$_3$) were also

23   considered in our calculations. CH$_3$OOH was estimated from observations of H$_2$O$_2$ made at

24   Dome C (mean value of 166 pptv, see Table 1) and assuming that it represents 40 ± 10 % of

25   H$_2$O$_2$ as reported by Frey et al. (2005] at the SP. For CH$_3$COCH$_3$ a typical mixing ratio of

26   130 ± 30 pptv was used on the basis of observations made at the SP (Hamer et al., 2007). For

27   CH$_3$COOH, Legrand et al. (2012) measured 60-70 pptv at Dome C between November and

28   February.

29   The calculated rates of radical sources and sinks are presented in Figures 5 and Table

30   2. Based on available measurements the major primary radical source is the photolysis of

31   HONO (1), with other net sources, namely, photolysis of HCHO (7), H$_2$O$_2$ (2), O$_3$ (3) and

CH$_3$CHO (8) being less important and contributing altogether less than 30% of the net radical production (the numbering of the reactions is according to the Table 2). It is important to emphasize here that, as detailed in section 2.2, the HONO data used in these calculations are thought to be biased by the presence of HO$_2$NO$_2$ (Legrand et al., this issue). Since the raw HONO concentration data cannot be accurately corrected for this measurement artefact, we consider in the following discussion (Section 3.4 and 3.5) several scenarios for HONO mixing ratios.

The recycling of OH and RO$_2$ radicals proceeds mainly via the reactions of HO$_2$ with NO (5) and of OH with CO (10) and CH$_4$ (11), with the production rate of OH from HO$_2$+NO being about half of the generation rate of OH via the photolysis of HONO. Although being less important, additional regeneration of RO$_2$ by the reactions of OH with HCHO, CH$_3$CHO, O$_3$ and H$_2$ (12-15) remain significant.

Net loss of the radicals proceeds mainly via the reactions OH+NO$_2$ (18), RO$_2$+NO$_2$ (24) and radical cross reactions OH+RO$_2$ (20) and RO$_2$ +RO$_2$ (25). Note that radical cross reactions become particularly important during the day when concentration of RO$_2$ is large (Table 2). Reactions of OH with NO, HONO, RO$_2$NO$_2$ and HNO$_3$ contribute together about 16% to the radical net losses. The contribution of the reaction of HO$_2$(H$_2$O) with NO$_2$ (Li et al., 2014) to the RO$_2$ losses is estimated with the rate constants given in Legrand et al. (this issue) to be less than 1%.

As the losses of OH and RO$_2$ via the reactions with NO$_2$ may be overestimated due to unknown interference in the NO$_2$ measurements (Frey et al., this issue) we also present in the Table 2 (values in parenthesis) the radical losses for [NO$_2$] estimated assuming PSS conditions for NO$_x$. In this case the net daytime radical losses are dominated by the radical cross reactions RO$_2$+RO$_2$ (25) and OH+RO$_2$ (20).

According to the above mechanism derived from the field observations, the sum of peroxy radicals RO$_2$ is composed predominantly of HO$_2$ and CH$_3$O$_2$, [RO$_2$] = [HO$_2$] + [CH$_3$O$_2$]. The ratio of [HO$_2$] to [RO$_2$] which was required for calculating the radical sources/sinks was estimated using steady-state calculations accounting for all identified sources and sinks of HO$_2$ and CH$_3$O$_2$. The resulting value of [HO$_2$]/[RO$_2$] is 0.67±0.05(1σ) and is close to the ratio of 0.73 estimated by only accounting for the production of RO$_2$ in the reactions of OH radical with CO and CH$_4$ and the loss of RO$_2$ via reactions of RO$_2$ with NO.

1   Concentrations of peroxy nitrates ($CH_3O_2NO_2$ and HO_2NO_2) involved in radical loss

2 reactions (see Table 2) were not measured at Dome C but were estimated assuming steady-

3 state conditions and accounting for their losses via photolysis, the reaction with OH, thermal

4 decomposition and a surface deposition of 7×10^{-5} s^{-1} (Slusher et al., 2002). The calculated

5 mixing ratios of HO_2NO_2 and $CH_3O_2NO_2$ were ~80 pptv and ~20 pptv, respectively. These

6 mixing ratios of HO_2NO_2 are somewhat higher than [HO_2NO_2] of 40-60 pptv observed at the

7 South Pole (Slusher et al., 2010) under conditions of significantly lower [NO_2] (estimated at

8 SP from NO observations assuming steady-state). Assuming the steady-state NO_2

9 concentrations at Dome C the estimated mixing ratios of HO_2NO_2 and $CH_3O_2NO_2$, are

10 significantly lower: ~10 pptv and ~3 pptv, respectively. In the work presented here the

11 calculated steady-state concentrations of peroxy nitrates were used to estimate the effective

12 loss rates of RO_2 radicals in the reactions with NO_2 by accounting for the regeneration of RO_2

13 via RO_2NO_2 thermal decomposition.

14   The mechanism presented above of the radical production and loss is supported by

15 examination of specific correlations. The major sources of OH radical, both the photolysis of

16 HONO and the recycling from HO_2, are expected to correlate with photolysis rates. Hence,

17 the observed close to linear correlation between [OH] and $J(NO_2)$ or $J(HONO)$ (Figures 3)

18 tends to support the importance of these two mechanisms of the production of OH radical.

19 However, the correlation of [OH] with $J(NO_2)$ explains only about 60% of [OH] variability,

20 while an additional source of [OH] variability may come from the variability of [HONO]

21 and/or [NO] as it can be seen from Figure 3. To account for the variability of [HONO] and

22 [NO], in Figure 6 we plotted [OH] against production rates of OH radical via photolysis of

23 HONO, (P_{HONO}), and via reaction of HO_2 with NO, (P_{HO2+NO}). The variability of P_{HO2+NO} and

24 P_{HONO} then explain ~80% and ~60% of the variability of OH, respectively.

25 **3.3   Photochemical budget of radicals**

26   According to the calculated sinks of OH and RO_2 radicals their lifetimes were less than

27 3 s and 100 s, respectively. The time scales for the variability of atmospheric parameters at

28 Dome C (boundary layer height and vertical diffusivity, solar radiation, NOx concentration

29 etc.) were typically significantly larger, more than 10 minutes. Hence, assuming validity of a

30 steady state approximation for OH and RO_2, their sources and sinks should be balanced.

31 However, as shown in Figure 5 and Table 2, on the basis of observations the sum of the

32 radical production rates exceeds by about (40-90)% and 25% the sum of loss rates for OH and

1   RO_2 radicals, respectively. Considering the primary sources and net sinks of the sum of OH

2   and peroxy radicals, the measured primary radical production is larger than their measured

3   total removal rate by a factor of 2 and 3 for midnight and noon times, respectively.

4   A similar result of the budget analysis follows from the comparison of the net OH and

5   RO_2 production rates, i.e. from the difference of the sum of their primary sources and the sum

6   of their net removal, and the total rate of the radical recycling. Under steady state conditions

7   the net production (or removal) rate of OH, $P_{pr}^{net}(OH)$, should be compensated by the net

8   removal (or production) rate of RO_2, $-P_{pr}^{net}(RO_2)$, and equal to the net recycling rate of OH to

9   RO_2 (or RO_2 to OH), $R^{net}(OH \rightarrow RO_2)$, (see Table 2):

10        $P_{pr}^{net}(OH) = R^{net}(OH \rightarrow RO_2) = -P_{pr}^{net}(RO_2)$

11   However, as seen in Table 2, according to the field measurements the net primary production

12   rate of OH significantly exceeds both the OH to RO_2 recycling and the net RO_2 removal rates.

13   At the same time, the net conversion rate of OH to RO_2 is not compensated by the measured

14   net removal rate of RO_2. This interpretation shows in a different way the same result as Figure

15   5: for both OH and RO_2 radicals the measured radical production rate exceeds their loss rate,

16   although for RO_2 the difference is less significant.

17   The observed imbalance between radical production and loss could result from

18   underestimated or unaccounted radical losses, as well as from overestimated radical sources.

19   As the main radical loss processes identified at Dome C were the reactions of radicals with

20   NO_2 and radical cross reactions the underestimation of the radical losses could be related to

21   an underestimation of measured concentration of NO_2 and/or concentrations of OH and RO_2

22   radicals. The underestimation of the radical concentrations by a factor of 2 is well outside the

23   estimated uncertainties for the measurements of OH and RO_2, although we can not completely

24   exclude some unknown error in the radical calibration procedure.

25   Considering the possibility of the underestimation of the concentration of NO_2,

26   sensitivity analysis shows that increasing of the concentrations of NO_2 by a factor of ~3

27   would result in a fair agreement of the model with the observations. However, as the observed

28     $[NO_2]/[NO]$ ratios at Dome C are already very high it is very unlikely that measured NO_2 was

29   underestimated. As discussed in Frey et al., (2013, this issue) the ratios of $[NO_2]/[NO]$

30   observed at Dome C are not consistent with other observations available at Dome C.

31   Accounting for the photolysis of NO_2 and conversion of NO to NO_2 in the reactions with

32   measured $[RO_2]$ and $[O_3]$ results in the ratio of $[NO_2]$ to $[NO]$ about a factor of 7 lower

compared to the measured values suggesting that there is a missing mechanism of the conversion of NO to NO_2. An explanation evoking an underestimation of the measured RO_2 can be excluded, because the concentrations of RO_2 radicals needed to explain the observed ratio of $[NO_2]/[NO]$ would be a factor of 20 larger than measured. Another possibility would be an additional conversion of NO to NO_2 in presence of halogens (i.g., ClO, BrO, IO) as was found at other polar sites, e.g at the coastal site of Halley (Bauguitte et al., 2012). However, to explain the observed ratio of $[NO_2]/[NO]$ at Dome C very large concentration of halogen species would be required, about 60 pptv in case of BrO and even higher for ClO. Such a large halogen mixing ratio is contradicted by measurements of BrO at Dome C, i.e. Frey et al., (this issue) report the BL mixing ratios of BrO of ~2 pptv. Hence, we conclude that either there is some unknown mechanism of NO to NO_2 conversion, or there was some interference affecting the NO_x measurements.

The analysis performed here of the radical chemistry at Dome C could be affected in both cases: the missing NO_x chemistry could interfere with chemistry involving OH and RO_2, i.e. by shifting the ratio $[RO_2]/[OH]$ towards OH, like in the case of efficient halogen chemistry at Summit, Greenland (Liao et al., 2011), while biased measurements of NO_x could affect the calculated radical losses and interconversion rates. Further speculations about possible impact of an unknown NO_x regulating mechanism on the OH and RO_2 chemistry are not feasible at this stage. Concerning possible interference in NO_x measurements, any correction consisting in a reduction of NO_2 would result in weaker radical losses and, hence, even larger overestimation of the radical sources. As shown in Table 2 the assumption of steady-state NO_2 concentrations lead to a significant overestimation of the net radical production for RO_2 and (RO_2+OH) even when neglecting net OH production by the photolysis of HONO. For OH budget, neglecting the net OH production by the HONO photolysis would lead to an underestimation of the OH production.

Considering the possibility of some overestimation of the OH radical production rate and independent of discussions carried out elsewhere (Legrand et al. this issue), one can see from the Figure 5 and Table 2 that among all the measured radical sources only the photolysis of HONO is large enough to explain, in case of its overestimation, the observed misbalance. In the following section we compare the observed concentrations of OH and RO_2 with model predictions to test the sensitivity of the modelled [OH] and $[RO_2]$ to the concentration of HONO.

3.4 Comparison with 0-D model: sensitivity to HONO

The simulations of concentration profiles of OH and RO_2 were conducted with different constraints on the concentration of HONO: taken as measured by LOPAP, the LOPAP measurements reduced by factors 2, 4, and estimated accounting for HONO production in HO+NO and HONO removal by photolysis assuming PSS conditions. The calculations were constrained with measured concentrations of NO_2 unless specifically stated that PSS derived NO_2 were used. The modelled concentrations of OH and RO_2 radicals are presented in Figures 7 and 8. Accounting for all radical sources including the photolysis of HONO leads to about a factor of 2 overestimation for modelled $[RO_2]$ and $[OH]$ with moderate correlation of the calculated and observed concentrations of OH and RO_2 radicals. Assuming HONO at PSS leads to an underestimation of $[OH]$ and $[RO_2]$ with a ratio of modelled to observed concentrations (M/O) of about 0.5 and a distinct difference between modelled and observed diurnal profiles (Figure 8), with better agreement during the daytime. As shown in Figure 8 the M/O for OH, RO_2 and their ratio become close to 1 by decreasing [HONO] from the measured to concentrations reduced by a factor of 4.

Similar to the approach adopted at the SP (e.g., Davis et al., 2004) we have tested the model assuming PSS HONO concentrations and using concentrations of NO_2 calculated by assuming photostationary ratio of $[NO_2]/[NO]$ calculated from the observed concentrations of NO, O_3 and RO_2. In this case, similar to the SP results, we obtain quite a good description for $[OH]$, although with up to a factor of 1.5 overestimation of $[RO_2]$ and $[RO_2]/[OH]$ ratio at noon (Figure 8).

Another insight on the relationship between the calculated concentrations of radicals and [HONO] can be gained by comparing the dependencies of observed and calculated $[OH]$ and $[RO_2]$ normalised by $J(NO_2)$ on [NO] (Figure 4). The model clearly shows that neglecting HONO photolysis and using constraints by measured concentrations of NO_x leads to a clear disagreement with observations. In this case, the calculated roll-off of normalised $[OH]$ starts at a mixing ratio of NO of about 50 pptv (Figures 4a) as a consequence of fast losses due to large $[NO_2]$ and the lack of additional OH production at higher concentrations of NO_x. When it is assumed that measurements of HONO are correct, $[OH]$ and $[RO_2]$ are overestimated by a factor of almost two in the whole range of observed [NO]. A better description by the model is achieved either when reducing the HONO concentrations by a factor of 4 or by neglecting HONO and using $[NO_2]$ calculated assuming PSS for NO_x (see also Figure 8). In the latter

1   case, the model underestimates the concentrations of radicals by 30-40% at large [NO],

2   although the number of observations at large concentrations of NO (>200 pptv) is limited.

3   Considering diurnal profiles of the M/O ratio presented in Figure 8 one can see that

4   although reducing the production rate of OH from the photolysis of HONO by reducing the

5   concentration of HONO improves the agreement between the model and the observations, the

6   diurnal profiles of the M/O ratio become more distinct indicating that a simple reduction of

7   [HONO] cannot provide a satisfactory description for the diurnal concentration profiles of OH

8   and RO_2. Thus, either some chemical mechanism is missing in the model and its effect on the

9   M/O ratio becomes stronger at reduced rates of OH production or, the overestimation of the

10 OH production rate is dependent on time of day (see discussion of effects related to BL

11 diffusivity in Section 3.5). In fact, median values of the time-dependent correction of

12 [HONO] necessary to provide agreement between calculated and observed radical

13 concentrations can be estimated by solving radical sources and losses balance equations for

14 the concentration of HONO. As shown in Figure 9, for the OH radical budget the balance is

15 achieved by reducing P_{HONO} by a factor of three during the day with a smaller correction

16 required during the night. Balancing the budget of primary production and net removal rates

17 of radicals requires neglecting the photolysis of HONO during the day and reducing it to a

18 quarter of its original value during the night time. According to a sensitivity analysis to

19 different measured parameters the calculated to observed [HONO] ratios,

20 $[HONO]_{calc}/[HONO]_{obs}$, are most sensitive to the concentrations of NO_2 and OH, RO_2

21 radicals. By assuming the PSS derived NO_2 concentrations, the balance for the OH radical

22 budget is achieved by reducing P_{HONO} by a factor of 5, while for RO_2 and the sum of RO_2 and

23 OH the radical production is overestimated even if the net source from HONO photolysis is

24 neglected.

25 **3.5   Comparison with 1D model**

26   It follows from the analysis presented above in Section 3.4 that the concentrations of

27 HONO observed at Dome C were probably too large and not compatible with the

28 measurements of OH and RO_2. Legrand et al. (this issue) give indications of possible

29 interference from HO_2NO_2 leading to an overestimation of the concentrations of HONO using

30 the LOPAP technique. According to Legrand et al. (this issue), about 100 pptv of HO_2NO_2

31 may result in interference equivalent to about 15 pptv of HONO. As the interference has not

1 yet been well characterized and, in addition, no measurements of HO_2NO_2 were available at
2 Dome C, a correction of HONO data at Dome C is not presently possible.

3   As an alternative approach, we have compared the concentrations of HONO derived
4 by examining the radical budget (Figure 9) with the calculations assuming HONO snow
5 emissions at Dome C estimated from the laboratory studies of Legrand et al. (this issue). By
6 irradiating the surface of snow collected at Concordia and simultaneously measuring the
7 concentrations of HONO and NO_x produced from the snow the authors found that HONO
8 mixing ratios in the experiment chamber outflow were roughly 30-50% of the mixing ratio of
9 NO_x, depending on snow temperature. Under temperature conditions encountered at Dome C
10 the HONO/NO_x ratio ranged from 0.57 during the day (at -25°C) and 0.3 at night (at -35°C).
11 Applying this ratio to the NO_x snow emission flux at Dome C, derived from the NO_x vertical
12 gradients measured during the OPAL campaign by Frey et al. (this issue), Legrand et al. (this
13 issue) estimated a HONO flux at Dome C ranging from 0.2×10^9 molecules cm^{-2} s^{-1} at night to
14 1.5×10^9 molecules cm^{-2} s^{-1} at noon. These fluxes of HONO were used in the work described
15 here to estimate the concentrations of HONO at different heights above the snow using the 1D
16 chemistry-transport box model (section 2.3) with turbulent vertical transport and a simplified
17 chemistry scheme including HONO production via the snow emissions only and HONO
18 removal via photolysis. Formation of HONO in the reaction OH+NO contributing less than
19 10% to the concentration of HONO resulting from the snow emissions was neglected in the
20 present 1D calculations. Another gas-phase source of HONO via reaction of $HO_2(H_2O)$
21 complex with NO_2 was recently proposed by Li et al. (2014). Owing to low temperatures at
22 Dome C the contribution of this source to [HONO] is estimated to be less than 2-3% (Legrand
23 et al., this issue) and it was also neglected in the 1D model.

24   The results of the 1D calculations are shown in Figure 10 where the median diurnal
25 profiles of emission fluxes, boundary layer heights and simulated mixing ratios of HONO at
26 1m and 3m are shown for the period from 19th December to 5th January. Figure 10 shows that
27 the difference of HONO mixing ratios at 1m and 3m does not exceed 30% and, hence, the
28 vertical gradient of [HONO] and measurements of [OH] and [HONO] at different heights, 1m
29 and 3m, respectively, can only partly explain the overestimation of OH production from
30 HONO. This conclusion does not depend on the strength of HONO flux used in the model
31 because the relative difference between concentrations of HONO at different heights above

1   the snowpack is determined only by the diffusivity of the boundary layer and the lifetime of

2   HONO.

3   The HONO mixing ratio-time profiles calculated with the 1D model are compared in

4   Figure 10 with the HONO profiles resulting from analysis of the radical budgets. The levels

5   of HONO derived from the OH budget with measured NO_2 are about 10 pptv higher than the

6   HONO values obtained using PSS NO_2 concentrations. In both cases the HONO mixing ratios

7   derived from the OH budget are in reasonable agreement with [HONO] predicted by the 1D

8   model (within 5 pptv). The 1D model reproduces also the diurnal HONO concentration

9   profile with a minimum during the day and larger concentration of HONO in the evening

10   resulting from interplay between emission rate and BL height variability (Legrand et al.,

11   2013). For the concentrations of HONO derived from the $OH+RO_2$ budget with measured

12   NO_2 the model significantly underestimates the derived from the budget daytime [HONO] but

13   provides better agreement for the night and reproduces general temporal trend of HONO

14   variability. The concentrations of HONO derived from the $OH+RO_2$ budget with steady-state

15   [NO_2] are negative (about -8 ppt during the day) and not presented in Figure 10.

16   **3.6   Ozone production**

17   The RO_2 and NO measurements made at Dome C were used to estimate local boundary

18   layer ozone production. As seen in Figure 11, the peak calculated ozone production rate

19   ($P(O_3)$) is about 0.3 ppbv h^{-1} during daytime (using the measurements of RO_2 at 3 m, NO at

20   4 m above the snowpack and assuming $P(O_3)$ equal to NO_2 production rate in the reaction of

21   RO_2 with NO). The production rate is in fairly good agreement with the previous estimation

22   of 0.2 ppbv h^{-1} derived from examination of diurnal changes in the concentration of ozone

23   (Legrand et al., 2009). The integrated 24h production of ozone reaches 4.7 ppbv d^{-1} at Dome

24   C and is similar to the one calculated for the SP where the daily production of ozone was

25   estimated from a model using measured concentrations of NO and OH to be of 2.2-3.6 ppbv

26   d^{-1} for ISCAT 1998 (Crawford et al., 2001) and 3.2-4.8 ppbv d^{-1} for ISCAT 2000 (Chen et al.,

27   2004).

28   It has to be emphasized with respect to the previous discussion of the ratio [NO_2]/[NO]

29   observed at Dome C that if the concentration of RO_2 radical was as large as needed to explain

30   the observed [NO_2]/[NO] ratio, the corresponding production rate of ozone would be as large

1   as 100 ppbv d^{-1} and would strongly conflict with observed diurnal change of ozone (see

2   Figure 3 in Legrand et al. (this issue).

3

4.   Conclusions

5   Concentrations of hydroxyl radicals and the sum of peroxy radicals, RO$_2$, have been

6   measured for the first time on the East Antarctic Plateau at the Concordia station (Dome C).

7   The concentrations of OH and RO$_2$ radicals were found to be comparable to those observed

8   previously at the South Pole (Mauldin et al., 2001, 2004, 2010) confirming that the elevated

9   oxidative capacity found at the SP is not unique but a common characteristic of near-surface

10   atmospheric layer for a large part of the high Antarctic plateau.

11   Similar to the findings at the SP the major explanation for the large concentrations of

12   OH radical at Dome C was found to be the large concentrations of NO (Frey et al., 2013, Frey

13   et al., this issue) leading to fast recycling of peroxy radicals to OH radicals. Also, similarly to

14   the SP, the variability of the concentration of NO$_x$ plays a major role in controlling the

15   variability of radicals (OH and RO$_2$) at Dome C. In contrast to the SP, where there is no

16   diurnal variation of solar radiation, and where radical levels are controlled by the

17   concentrations of NO mostly via changing boundary layer properties (Neff et al., 2008), [OH]

18   and [RO$_2$] at Dome C show strong diurnal variability correlating with the solar cycle, which

19   in turn controls the rate of radical production and the rate of interconversion of OH and RO$_2$

20   radicals.

21   The large concentrations of radicals and NO result in ozone production in the BL at

22   Dome C with a production rate of 0.1-0.3 ppb h^{-1}, similar to that observed at the SP.

23   The major primary sources of radicals in the atmosphere at Dome C are represented by

24   the photolysis of HONO, HCHO, CH$_3$CHO and H$_2$O$_2$, (in order of decreasing significance),

25   with photolysis of HONO deduced from measurements of HONO contributing for about 75%

26   of total primary production of radicals. The main net losses of radicals are represented by

27   their reactions with NO$_2$ and cross radical reactions. However, it is found, that these results

28   are inconsistent with observations of radicals leading to about a factor of 2 overestimation of

29   the concentrations of RO$_2$ and OH radicals. At the same time, neglecting the production of

30   OH radical from the photolysis of HONO results in about a factor of 2 underestimation of the

31   measured concentrations of radicals. Based on 0D modelling, to explain the observations of

1 OH and RO$_2$ radicals in this case an additional source of OH equivalent to about 25% of

2 measured photolysis of HONO is required. Similar result follows from analysis of the

3 photochemical budget of the OH radicals for which the balance is achieved by reducing

4 P$_{HONO}$ by a factor of three.

5 The conclusions based on the radical budget analysis and 0D modelling using the measured

6 concentrations of NO and NO$_2$ may be significantly biased because the chemical mechanism

7 derived from the available field observations at Dome C is inconsistent with observed large

8 ratios of [NO$_2$] to [NO]. Assuming that measured NO$_2$ mixing ratios were overestimated due

9 to unknown interference and using instead [NO$_2$] estimated assuming steady-state results in

10 lower radical losses and, hence, stronger overestimation of the radical production. In this case,

11 based on the analysis of the radical budgets the observed concentrations of OH radicals are

12 consistent with the levels of HONO corresponding to about (15-20)% of the measured values,

13 while for the sum of the radicals the radical production is overestimated even neglecting the

14 net OH source from the photolysis of HONO. Based on 0D modelling steady-state derived

15 NO$_2$, the measured OH concentrations are in agreement with steady-state HONO mixing

16 ratios (about 1-2 pptv), while the concentrations of RO$_2$ radicals are overestimated by about

17 50% even neglecting the net radical production by the photolysis of HONO.

18 Hence, in both cases corresponding to the measured or the PSS derived concentrations

19 of NO$_2$ the calculations, 0D modelling or budget analysis, overestimate the OH and RO$_2$

20 concentrations. If this inconsistency is due to an overestimation of the concentrations of

21 HONO, the degree of the overestimation depends on the concentrations of NO$_2$ used in the

22 calculations. Using the measured NO$_2$ results in an overestimation of HONO by a factor of 3-

23 4. If the concentrations of NO$_2$ are estimated assuming steady-state conditions the net radical

24 production from the HONO photolysis should be reduced by a factor of 5 or completely

25 removed based on the budget of OH or 0D modelling, respectively.

26 Assuming that HONO at Dome C originates from snow emissions with the emission

27 strength evaluated by Legrand et al., (this issue) we obtain from a 1D model the

28 concentrations of HONO corresponding to about 20-30% of measured [HONO] and the

29 diurnal concentration profiles of HONO consistent with those calculated from the budget

30 analysis of OH radicals with the concentrations of NO$_2$ either calculated assuming PSS or

31 taken from the measurements. We suggest that an explanation for the overestimation of

32 radical production could be an overestimation of measured concentration of HONO, which

may originate from the measurement interference from HO_2NO_2 affecting measurements of HONO by LOPAP (Legrand et al., this issue). Even with a factor of 4 reduction in the concentrations of HONO, the photolysis of HONO represents the major primary radical source at Dome C accounting for about 45% of primary radical production.

Considering the observed uncertainties in HONO and NO_x measurements we suggest that further studies of NO_x, HONO, peroxy nitrates (RO_2NO_2) and radical chemistry at Antarctic Plateau are required with specific efforts dedicated to increase the reliability of measurements (especially HONO and NO_2) under polar conditions.

References

Bauguitte, S. J. B., Bloss, W. J., Evans, M. J., Salmon, R. A., Anderson, P. S., Jones, A. E., Lee, J. D., Saiz-Lopez, A., Roscoe, H. K., Wolff, E. W., and Plane, J. M. C.: Summertime NOx measurements during the CHABLIS campaign: can source and sink estimates unravel observed diurnal cycles?, Atmos. Chem. Phys., 12, 989-1002, 2012.

Berresheim, H., Elste, T., Plass-Dulmer, C., Eisele, F. L., and Tanner, D. J.: Chemical ionization mass spectrometer for long-term measurements of atmospheric OH and H2SO4, Int. J. Mass Spectrom., 202, 91-109, 2000.

Chen, G., Davis, D., Crawford, J., Hutterli, L. M., Huey, L. G., Slusher, D., Mauldin, L., Eisele, F., Tanner, D., Dibb, J., Buhr, M., McConnell, J., Lefer, B., Shetter, R., Blake, D., Song, C. H., Lombardi, K., and Arnoldy, J.: A reassessment of HOx South Pole chemistry based on observations recorded during ISCAT 2000, Atmos. Environ., 38, 5451-5461, 2004.

Crawford, J. H., Davis, D. D., Chen, G., Buhr, M., Oltmans, S., Weller, R., Mauldin, L., Eisele, F., Shetter, R., Lefer, B., Arimoto, R., and Hogan, A.: Evidence for photochemical production of ozone at the South Pole surface, Geophys. Res. Lett., 28, 3641-3644, 2001.

Davis, D., Nowak, J. B., Chen, G., Buhr, M., Arimoto, R., Hogan, A., Eisele, F., Mauldin, L., Tanner, D., Shetter, R., Lefer, B., and McMurry, P.: Unexpected high levels of NO observed at South Pole, Geophys. Res. Lett., 28, 3625-3628, 2001.

Davis, D. D., Eisele, F., Chen, G., Crawford, J., Huey, G., Tanner, D., Slusher, D., Mauldin, L., Oncley, S., Lenschow, D., Semmer, S., Shetter, R., Lefer, B., Arimoto, R., Hogan, A., Grube, P., Lazzara, M., Bandy, A., Thornton, D., Berresheim, H., Bingemer, H., Hutterli, M., McConnell, J., Bales, R., Dibb, J., Buhr, M., Park, J., McMurry, P., Swanson, A., Meinardi, S., and Blake, D.: An overview of ISCAT 2000, Atmos. Environ., 38, 5363-5373, 2004.

Davis, D. D., Seelig, J., Huey, G., Crawford, J., Chen, G., Wang, Y. H., Buhr, M., Helmig, D., Neff, W., Blake, D., Arimoto, R., and Eisele, F.: A reassessment of Antarctic plateau reactive nitrogen based on ANTO 2003 airborne and ground based measurements, Atmos. Environ., 42, 2831-2848, 2008.

Dibb, J. E., Huey, L. G., Slusher, D. L., and Tanner, D. J.: Soluble reactive nitrogen oxides at South Pole during ISCAT 2000, Atmos. Environ., 38, 5399-5409, 2004.

1 Dusanter, S., Vimal, D., and Stevens, P. S.: Technical note: Measuring tropospheric OH and
2 HO2 by laser-induced fluorescence at low pressure. A comparison of calibration techniques,
3 Atmos. Chem. Phys., 8, 321-340, 2008.

4 Eisele, F. L. and Tanner, D. J.: Ion-Assisted Tropospheric OH Measurements, J. Geophys.
5 Res. Atmos., 96, 9295-9308, 1991.

6 Eisele, F., Davis, D. D., Helmig, D., Oltmans, S. J., Neff, W., Huey, G., Tanner, D., Chen, G.,
7 Crawford, J., Arimoto, R., Buhr, M., Mauldin, L., Hutterli, M., Dibb, J., Blake, D., Brooks, S.
8 B., Johnson, B., Roberts, J. M., Wang, Y. H., Tan, D., and Flocke, F.: Antarctic Tropospheric
9 Chemistry Investigation (ANTCI) 2003 overview, Atmospheric Environment, 42, 2749-2761,
10 2008.

11 Faloona, I. C., Tan, D., Lesher, R. L., Hazen, N. L., Frame, C. L., Simpas, J. B., Harder, H.,
12 Martinez, M., Di Carlo, P., Ren, X. R., and Brune, W. H.: A laser-induced fluorescence
13 instrument for detecting tropospheric OH and HO2: Characteristics and calibration, J. Atmos.
14 Chem., 47, 139-167, 2004.

15 France, J. L., King, M. D., Frey, M. M., Erbland, J., Picard, G., Preunkert, S., MacArthur, A.,
16 and Savarino, J.: Snow optical properties at Dome C (Concordia), Antarctica; implications for
17 snow emissions and snow chemistry of reactive nitrogen, Atmos. Chem. and Phys., 11, 9787-
18 9801, 2011.

19 Frey, M. M., Stewart, R. W., McConnell, J. R., and Bales, R. C.: Atmospheric hydroperoxides
20 in West Antarctica: Links to stratospheric ozone and atmospheric oxidation capacity, J.
21 Geophys. Res. Atmos., 110, 2005.

22 Frey, M. M., Brough, N., France, J. L., Anderson, P. S., Traulle, O., King, M. D., Jones, A.
23 E., Wolff, E. W., and Savarino, J.: The diurnal variability of atmospheric nitrogen oxides (NO
24 and NO2) above the Antarctic Plateau driven by atmospheric stability and snow emissions,
25 Atmos. Chem. Phys., 13, 3045-3062, 2013.

26 Fuchs, H., Holland, F., and Hofzumahaus, A.: Measurement of tropospheric RO2 and HO2
27 radicals by a laser-induced fluorescence instrument, Rev. of Sci. Instrum., 79, 2008.

28 Gallée, H. and Gorodetskaya, I.: Validation of a limited area model over Dome C, Antarctic
29 Plateau, during winter, 34, 61–72, Clim. Dyn., doi:10.1007/s00382-008-0499-y, 2008.

Grannas, A. M., Jones, A. E., Dibb, J., Ammann, M., Anastasio, C., Beine, H. J., Bergin, M., Bottenheim, J., Boxe, C. S., Carver, G., Chen, G., Crawford, J. H., Domine, F., Frey, M. M., Guzman, M. I., Heard, D. E., Helmig, D., Hoffmann, M. R., Honrath, R. E., Huey, L. G., Hutterli, M., Jacobi, H. W., Klan, P., Lefer, B., McConnell, J., Plane, J., Sander, R., Savarino, J., Shepson, P. B., Simpson, W. R., Sodeau, J. R., von Glasow, R., Weller, R., Wolff, E. W., and Zhu, T.: An overview of snow photochemistry: evidence, mechanisms and impacts, Atmos. Chem. Phys., 7, 4329-4373, 2007.

Hamer, P. D., Shallcross, D. E. and Frey, M. M.: Modelling the impact of oxygenated VOC and meteorology upon the boundary layer photochemistry at the South Pole, Atmos. Sci. Let., 8, 14-20, 2007.

Hanke, M., Uecker, J., Reiner, T., and Arnold, F.: Atmospheric peroxy radicals: ROXMAS, a new mass-spectrometric methodology for speciated measurements of HO2 and Sigma RO2 and first results, Int. J. Mass Spectrom., 213, 91-99, 2002.

Heard, D. E. and Pilling, M. J.: Measurement of OH and HO2 in the troposphere, Chem. Rev., 103, 5163-5198, 2003.

Heland, J., Kleffmann, J., Kurtenbach, R., and Wiesen, P. : A new instrument to measure gaseous nitrous acid (HONO) in the atmosphere, Environ. Sci. Technol., 35(15), 3207-3212, doi:10.1021/es000303t, 2001.

Honrath, R. E., Peterson, M. C., Guo, S., Dibb, J. E., Shepson, P. B., and Campbell, B.: Evidence of NOx production within or upon ice particles in the Greenland snowpack, Geoph. Res. Lett., 26, 695-698, 1999.

Jäkel, E., Wendisch, M., Blumthaler, M., Schmitt, R., and Webb, A. R.: (2007). "A CCD Spectroradiometer for Ultraviolet Actinic Radiation Measurements." J. Atmos. Oceanic Technol. 24(3), 449-462.

Jenkin, M. E., Saunders, S. M., and Pilling, M. J.: The tropospheric degradation of volatile organic compounds: A protocol for mechanism development, Atmos. Environ., 31, 81-104, 1997.

Jones, A.E., Weller, R., Anderson, P.S., Jacobi, H.W., Wolff, E.W., Schrems, O., and Miller, H. : Measurements of NOx emissions from the Antarctic snowpack, Geophys. Res. Lett., 28, 1499–1502, 2001.

1   Kerbrat, M., Legrand, M., Preunkert, S., Gallee, H., and Kleffmann, J.: Nitrous acid at

2   Concordia (inland site) and Dumont d'Urville (coastal site), East Antarctica, J. Geophys. Res.

3   Atmos., 117, 2012.

4   King, J. C., Argentini, S. A., and Anderson, P. S.: Contrasts between the summertime surface

5   energy balance and boundary layer structure at Dome C and Halley stations, Antarctica, J.

6   Geophys. Res. Atmos., 111, D02105, doi:10.1029/2005JD006130, 2012.

7   Kleffmann, J., Heland, J., Kurtenbach, R., Lorzer, J., and Wiesen, P.: A new instrument

8   (LOPAP) for the detection of nitrous acid (HONO), Environ. Sci. Pollut. Res., (Sp. Iss. 4),

9   48–54, 2002.

10   Kukui, A., Ancellet, G., and Le Bras, G.: Chemical ionisation mass spectrometer for

11   measurements of OH and Peroxy radical concentrations in moderately polluted atmospheres,

12   J. Atmos. Chem., 61, 133-154, 2008.

13   Kukui, A., Legrand, M., Ancellet, G., Gros, V., Bekki, S., Sarda-Esteve, R., Loisil, R., and

14   Preunkert, S.: Measurements of OH and RO2 radicals at the coastal Antarctic site of Dumont

15   d'Urville (East Antarctica) in summer 2010-2011, J. Geophys. Res. Atmos., 117, 2012.

16   Legrand, M., Preunkert, S., Jourdain, B., Gallee, H., Goutail, F., Weller, R., and Savarino, J.:

17   Year-round record of surface ozone at coastal (Dumont d'Urville) and inland (Concordia) sites

18   in East Antarctica, J. Geophys. Res. Atmos., 114, 2009.

19   Legrand, M., Gros, V., Preunkert, S., Sarda-Estève, R., Thierry, A.-M., Pépy, G., and

20   Jourdain, B.: A reassessment of the budget of formic and acetic acids in the boundary layer at

21   Dumont d'Urville (coastal Antarctica): The role of penguin emissions on the budget of several

22   oxygenated volatile organic compounds, J. Geophys. Res. Atmos., 117, D06308,

23   doi:10.1029/2011JD017102, 2012.

24   Legrand, M., Preunkert, S., Frey, M., Bartels-Rausch, T., Kukui, A., King, M., Kerbrat, M,

25   Jourdain, B., and Savarino, J: High atmospheric levels of nitrous acid at Concordia (East

26   Antarctic plateau) in summer: A strong source from surface snow ?, Atmos. Chem. Phys., this

27   issue.

28   Li, X., Rohrer, F., Hofzumahaus, A., Brauers, T., Häseler, R., Bohn, B., Broch, S., Fuchs, H.,

29   Gomm, S., Holland, F., Jäger, J., Kaiser, J., Keutsch, F. N., Lohse, I., Lu, K., Tillmann, R.,

30   Wegener, R., Wolfe, G. M., Mentel, T. F., Kiendler-Scharr, A., and Wahner, A.: Missing Gas-

Phase Source of HONO Inferred from Zeppelin Measurements in the Troposphere, Science, 344, 292-296, 2014.

Liao, J., Huey, L. G., Tanner, D. J., Brough, N., Brooks, S., Dibb, J. E., Stutz, J., Thomas, J. L., Lefer, B., Haman, C., and Gorham, K.: Observations of hydroxyl and peroxy radicals and the impact of BrO at Summit, Greenland in 2007 and 2008, Atmos. Chem. Phys., 11, 8577-8591, 2011.

Madronich, S.: Photodissociation in the atmosphere 1. Actinic flux and the effects of ground reflectance and clouds, J. Geophys. Res. 92(D8), 9740-9752, 1987.

Madronich, S. and Flocke, S.: The role of solar radiation in atmospheric chemistry, in Handbook of Environmental Chemistry (P. Boule, ed.), Springer_Verlag, Heidelberg, pp. 1-26, 1998.

Mauldin, R. L., Eisele, F. L., Tanner, D. J., Kosciuch, E., Shetter, R., Lefer, B., Hall, S. R., Nowak, J. B., Buhr, M., Chen, G., Wang, P., and Davis, D.: Measurements of OH, H2SO4, and MSA at the South Pole during ISCAT, Geophys. Res. Lett., 28, 3629-3632, 2001.

Mauldin, R. L., Kosciuch, E., Henry, B., Eisele, F. L., Shetter, R., Lefer, B., Chen, G., Davis, D., Huey, G., and Tanner, D.: Measurements of OH, HO2+RO2, H2SO4, and MSA at the south pole during ISCAT 2000, Atmos. Environ., 38, 5423-5437, 2004.

Mauldin, R., Kosciuch, E., Eisele, F., Huey, G., Tanner, D., Sjostedt, S., Blake, D., Chen, G., Crawford, J., and Davis, D.: South Pole Antarctica observations and modeling results: New insights on HOx radical and sulfur chemistry, Atmos. Environ., 44, 572-581, 2010.

Michoud, V., Kukui, A., Camredon, M., Colomb, A., Borbon, A., Miet, K., Aumont, B., Beekmann, M., Durand-Jolibois, R., Perrier, S., Zapf, P., Siour, G., Ait-Helal, W., Locoge, N., Sauvage, S., Afif, C., Gros, V., Furger, M., Ancellet, G., and Doussin, J. F.: Radical budget analysis in a suburban European site during the MEGAPOLI summer field campaign, Atmos. Chem. Phys., 12, 11951-11974, 2012.

Neff, W., Helmig, D., Grachev, A., and Davis, D.: A study of boundary layer behavior associated with high NO concentrations at the South Pole using a minisodar, tethered balloons and sonic anemometer, Atmos. Environ., 42, 2762-2779, 2008.

Novelli, P. C. and Masarie, K. A.: Atmospheric Carbon Monoxide Dry Air Mole Fractions from the NOAA ESRL Carbon Cycle Cooperative Global Air Sampling Network, 1988-2012, Version: 2013-06-18, Path: ftp://aftp.cmdl.noaa.gov/data/trace_gases/co/flask/surface/, 2013.

Preunkert, S., Ancellet, G., Legrand, M., Kukui, A., Kerbrat, M., Sarda-Esteve, R., Gros, V., and Jourdain, B.: Oxidant Production over Antarctic Land and its Export (OPALE) project: An overview of the 2010-2011 summer campaign, J. Geophys. Res. Atmos., 117, 2012.

Preunkert, S., Legrand, M., Pépy, G., Gallée, H., Jones, A., and Jourdain, B.: The atmospheric HCHO budget at Dumont d'Urville (East Antarctica): Contribution of photochemical gas-phase production versus snow emissions, J. Geophys. Res. Atmos., 118, doi:10.1002/2013JD019864, in press, 2014.

Preunkert, S., Legrand, M., Jourdain, B., Kukui, A., Gallée, H., and Frey, M.: Formaldehyde in air, snow, and interstitial air at Concordia (East Antarctic plateau), Atmos. Chem. Phys., this issue.

Reiner, T., Hanke, M., and Arnold, F.: Atmospheric peroxy radical measurements by ion molecule reaction mass spectrometry: A novel analytical method using amplifying chemical conversion to sulfuric acid, J. Geophys. Res. Atmos., 102, 1311-1326, 1997.

Sander, S. P., Abbatt, J., Barker, J. R., Burkholder, J. B., Friedl, R. R., Golden, D. M., Huie, R. E., Kolb, C. E., Kurylo, M. J., Moortgat, G. K., Orkin, V. L., and Wine, P. H.: Chemical Kinetics and photochemical Data for Use in Atmospheric Studies, Evaluation No. 17, JPL Publication 10-6, Jet Propulsion Laboratory, Pasadena, 2011 http://jpldataeval.jpl.nasa.gov.

Saunders, S. M., Jenkin, M. E., Derwent, R. G., and Pilling, M. J.: Protocol for the development of the Master Chemical Mechanism, MCM v3 (Part A): tropospheric degradation of non-aromatic volatile organic compounds, Atmos. Chem. Phys., 3, 161-180, 2003.

Sjostedt, S. J., Huey, L. G., Tanner, D. J., Peischl, J., Chen, G., Dibb, J. E., Lefer, B., Hutterli, M. A., Beyersdorf, A. J., Blake, N. J., Blake, D. R., Sueper, D., Ryerson, T., Burkhart, J., and Stohl, A.: Observations of hydroxyl and the sum of peroxy radicals at Summit, Greenland during summer 2003, Atmos. Environ., 41, 5122-5137, 2007.

Slusher, D. L., Huey, L. G., Tanner, D. J., Chen, G., Davis, D. D., Buhr, M., Nowak, J. B., Eisele, F. L., Kosciuch, E., Mauldin, R. L., Lefer, B. L., Shetter, R. E., and Dibb, J. E.:

Measurements of pernitric acid at the South Pole during ISCAT 2000, Geophys. Res. Lett., 29, 2002.

Slusher, D. L., Neff, W. D., Kim, S., Huey, L. G., Wang, Y., Zeng, T., Tanner, D. J., Blake, D. R., Beyersdorf, A., Lefer, B. L., Crawford, J. H., Eisele, F. L., Mauldin, R. L., Kosciuch, E., Buhr, M. P., Wallace, H. W., and Davis, D. D.: Atmospheric chemistry results from the ANTCI 2005 Antarctic plateau airborne study, J. Geophys. Res. Atmos., 115, 2010.

Steele, L. P., Krummel, P. B. and Langenfelds, R. L.: Atmospheric H_2 concentrations from sites in the CSIRO Atmospheric Research GASLAB air sampling network (October 2002 version). In Trends: A Compendium of Data on Global Change, Carbon Dioxide Information Analysis Center, Oak Ridge National Laboratory, U.S. Department of Energy, Oak Ridge, TN, U.S.A., 2003.

Steele, L. P., Krummel, P. B. and Langenfelds, R. L.: Atmospheric CH_4 concentrations from sites in the CSIRO Atmospheric Research GASLAB air sampling network (October 2002 version). In Trends: A Compendium of Data on Global Change, Carbon Dioxide Information Analysis Center, Oak Ridge National Laboratory, U.S. Department of Energy, Oak Ridge, TN, U.S.A., 2002.

Tanner, D. J., Jefferson, A., and Eisele, F. L.: Selected ion chemical ionization mass spectrometric measurement of OH, J. Geophys. Res. Atmos., 102, 6415-6425, 1997.

Wang, Y. H., Choi, Y., Zeng, T., Davis, D., Buhr, M., Huey, L. G., and Neff, W.: Assessing the photochemical impact of snow NOx emissions over Antarctica during ANTCI 2003, Atmos. Environ., 41, 3944-3958, 2007.

1

Table 1. Comparison of measurements at Dome C and at the South Pole

	Dome C, 75.1° S / 123.3° E *19 Dec,2011 ÷ 10 Jan,2012*		SP, ISCAT 1998	SP, ISCAT 2000	SP, ANTCI 2003
	Median (range of median) values	Method (2σ uncertainty)	Median values (*Dec, 16-31*) [a]		
P, mb	645		688	692	695
T, °C	-29.6 (-35.8 ÷ -26.1)		-29.1	-27.6	-23.9
WS, m s^{-1}	3.1 (2.3÷4.5)		3.2	3.74	4.9
OH, 10^6 molecule cm^{-3}	3.1 (1.1÷5.0) 5.0 (at 12h, JO^{1}D=5×10^{-5}) 2.5 (at 5h, JO^{1}D=9×10^{-6}) 3.8 (at 19h, JO^{1}D=9×10^{-6})	CIMS (40% - 60%)	1.7	2.3	1.2
RO$_2$, 10^7 molecule cm^{-3}	9.9 (2.5÷17.0) 17.0 (at 12h, JO^{1}D=5×10^{-5}) 7.9 (at 5h, JO^{1}D=9×10^{-6}) 7.5 (at 19h, JO^{1}D=9×10^{-6})	CIMS (47% - 50%)	-	8.1	-
J(O^{1}D), 10^{-6} s^{-1}	13.4 (1.2 ÷ 49)	Spectroradiometer (MetCon …) (3% (JNO$_2$);6% (JO^{1}D))	8.9	8.5	8.5
J(NO$_2$), 10^{-2} s^{-1}	1.3 (0.4 ÷ 2.1)		1.0	1.1	0.8
O$_3$,ppb	23.7 (22÷25)	UV abs. (2%)	26.1	30	32
NO, ppt (1m)	77 (46÷134)	Chemiluminiscence (40%) [h]	237	88	*76*
NO$_2$, ppt (1m)	149 (110÷239) 16 (7-64) [i]	Photolytic conv., Chemiluminiscence (200%) [h]	*115* [b]	*44* [b]	*38* [b]
HONO , ppt	38 (27÷44)	LOPAP (5%)	-	28 (MC/IC)	4.9 (LIF, 10m) 51(MC/IC, 1m) [c] 7.3 (LIF, 10m) [c]
HCHO , ppt	131 (117÷153)	Fluorimetry , Aerolaser AL4021 (20%)	-	105	74
H$_2$O$_2$, ppt	166 (128÷228)	Fluorimetry, Aerolaser AL2021 (18%)	-	229	286
P(O$_3$), ppb day^{-1}	4.7 (0.04 ÷ 0.34, in ppb h^{-1}) [d]		2.2÷3.6 [e]	3.2÷4.8 [f]	1÷3.5 [g]

3

4   a) SP data from (Eisele et al., 2008), if no other reference

5   b) estimated assuming PSS ratio NO/NO$_2$=2 (Davis et al., 2004; Slusher et al., 2002);

6   c) median for 1-15 of December

7   d) calculated using the measured RO$_2$ and NO

8   e) Crawford et al., (2001)

9   f) Chen et al., (2004)

10   g) Davis et al., (2008)

11   h) median of relative 2σ errors

12   i) NO$_2$ estimated assuming photostationary steady-state conditions for NO$_x$

Table 2. Sources and sinks of OH and RO_2 radicals estimated from the measurements available at Dome C [*]

		median rate, 10^5 molecule $cm^{-3}s^{-1}$		
		daily	noon	midnight
	net OH sources			
1	$HONO + h\nu \rightarrow OH + NO$	14.2 (0.5)	21.8 (0.6)	4.7 (0.2)
2	$H_2O_2 + h\nu \rightarrow OH + OH$	0.9	2.1	0.1
3	$O_3 + h\nu \rightarrow O(^1D) \rightarrow OH + OH$	0.3	1.7	0.0
4	$CH_3OOH + h\nu \rightarrow HO_2 + OH$	0.2	0.4	0.0
	recycling $RO_2 \rightarrow OH$			
5	$HO_2 + NO \rightarrow OH + NO_2$	8.3	11.6	2.2
6	$HO_2 + O_3 \rightarrow OH + 2O_2$	0.4	0.6	0.1
	net RO_2 sources			
7	$HCHO + h\nu \rightarrow 2HO_2 + CO$	2.1	3.7	0.4
8	$CH_3CHO + h\nu \rightarrow HO_2 + CH_3O_2 + CO$	0.9	2.1	0.2
9	$CH_3OOH + h\nu \rightarrow HO_2 + OH$	0.2	0.4	0.03
	recycling $OH \rightarrow RO_2$			
10	$CO + OH \rightarrow HO_2 + CO_2$	5.9	7.8	1.9
11	$CH_4 + OH \rightarrow CH_3O_2 + H_2O$	2.3	3.3	0.7
12	$HCHO + OH \rightarrow HO_2 + CO$	1.0	1.1	0.3
13	$CH_3CHO + OH \rightarrow CH_3CO_3$	0.8	1.1	0.3
14	$O_3 + OH \rightarrow HO_2 + O_2$	0.6	0.7	0.2
15	$H_2 + OH \rightarrow HO_2 + H_2O$	0.5	0.8	0.2
16	$CH_3OOH + OH \rightarrow CH_3O_2 + H_2O$	0.3	0.5	0.1
17	$H_2O_2 + OH \rightarrow HO_2 + H_2O$	0.1	0.3	0.0
	net radical losses			
18	$OH + NO_2 \rightarrow HNO_3$	1.9 (0.3)	2.2 (0.3)	1.1 (0.3)
19	$OH + NO \rightarrow HONO$	0.5	0.6	0.2
20	$OH + RO_2 \rightarrow products$	0.4	1.0	0.0
21	$OH + RO_2NO_2 \rightarrow products$	0.4 (0.05)	0.5 (0.06)	0.1 (0.02)
22	$OH + HONO \rightarrow H_2O + NO_2$	0.1 (0.0)	0.2 (0.0)	0.1 (0.0)
23	$OH + HNO_3 \rightarrow H_2O + NO_3$ [a]	0.0	0.0	0.0
24	$RO_2 + NO_2 \rightarrow RO_2NO_2 \rightarrow products$	1.9 (0.3)	2.4 (0.3)	1.2 (0.3)
25	$RO_2 + RO_2 \rightarrow products$	0.7	2.1	0.1
26	$RO_2 + OH \rightarrow products$	0.4	1.0	0.0
	$\sum OH$ sources	24.2 ± 2.1 [b] (10.6 ± 0.2)	38.3 ± 3.2 (17.1±0.3)	7.1 ± 0.7 (4.3±0.1)
	$\sum OH$ losses	14.8 ± 4.6 (12.9±1.8)	20.3 ± 3.6 (17.9±2.2)	5.1 ± 1.2 (4.3±0.9)
	Δ	9.4 ± 5.0 (-2.4±2.7)	17.9 ± 4.8 (-0.8±3.8)	2.1 ± 1.4 (-1.7±1.2)
	$\sum RO_2$ sources	14.6 ± 1.8	21.9 ± 2.3	4.2 ± 0.9
	$\sum RO_2$ losses	11.7 ± 4.6 (10.2±2.1)	17.7 ± 7.2 (15.6±3.3)	3.5 ± 1.6 (2.7±0.8)
	Δ	2.9 ± 5.0 (4.4±2.8)	4.2 ± 7.6 (6.3±4.0)	0.7 ± 1.9 (1.5±1.2)
	$\sum RO_2$ and OH net sources	18.7 ± 0.6 (5.1±0.3)	32.3 ± 0.9 (11.1±0.7)	5.5 ± 0.1 (0.9±0.1)
	$\sum RO_2$ and OH net losses	6.4 ± 5.9 (3.0±0.8)	10.1 ± 7.1 (5.6±1.1)	2.7 ± 1.7 (1.1±0.4)
	Δ	12.3 ± 6.0 (2.1±0.9)	22.2 ± 7.2 (5.5±1.3)	2.7 ± 1.7 (-0.1±0.5)
	$P_{pr}^{net}(OH) = \sum net\ OHt\ sources - \sum net\ OH\ losses$	12.2 ± 4.2 (0.4±0.3)	21.4 ± 3.0 (2.7±0.5)	3.4 ± 0.8 (-0.3±0.2)
	$R_{net}(OH \rightarrow RO_2) = \sum(OH \rightarrow RO_2) - \sum(RO_2 \rightarrow OH)$	2.8 ± 2.7	3.5 ± 3.8	1.4 ± 1.1
	$P_{pr}^{net}(RO_2) = \sum net\ RO_2\ sources - \sum net\ RO_2\ losses$	0.15 ± 4.2 (1.7±0.8)	0.74 ± 6.6 (2.8±1.2)	-0.7 ± 1.5 (0.2±0.4)

[*] Values in parentheses correspond to NO_2 and HONO estimated assuming PSS

a) HNO_3 of (100±30) ppt was assumed (Slusher et al., 2010)

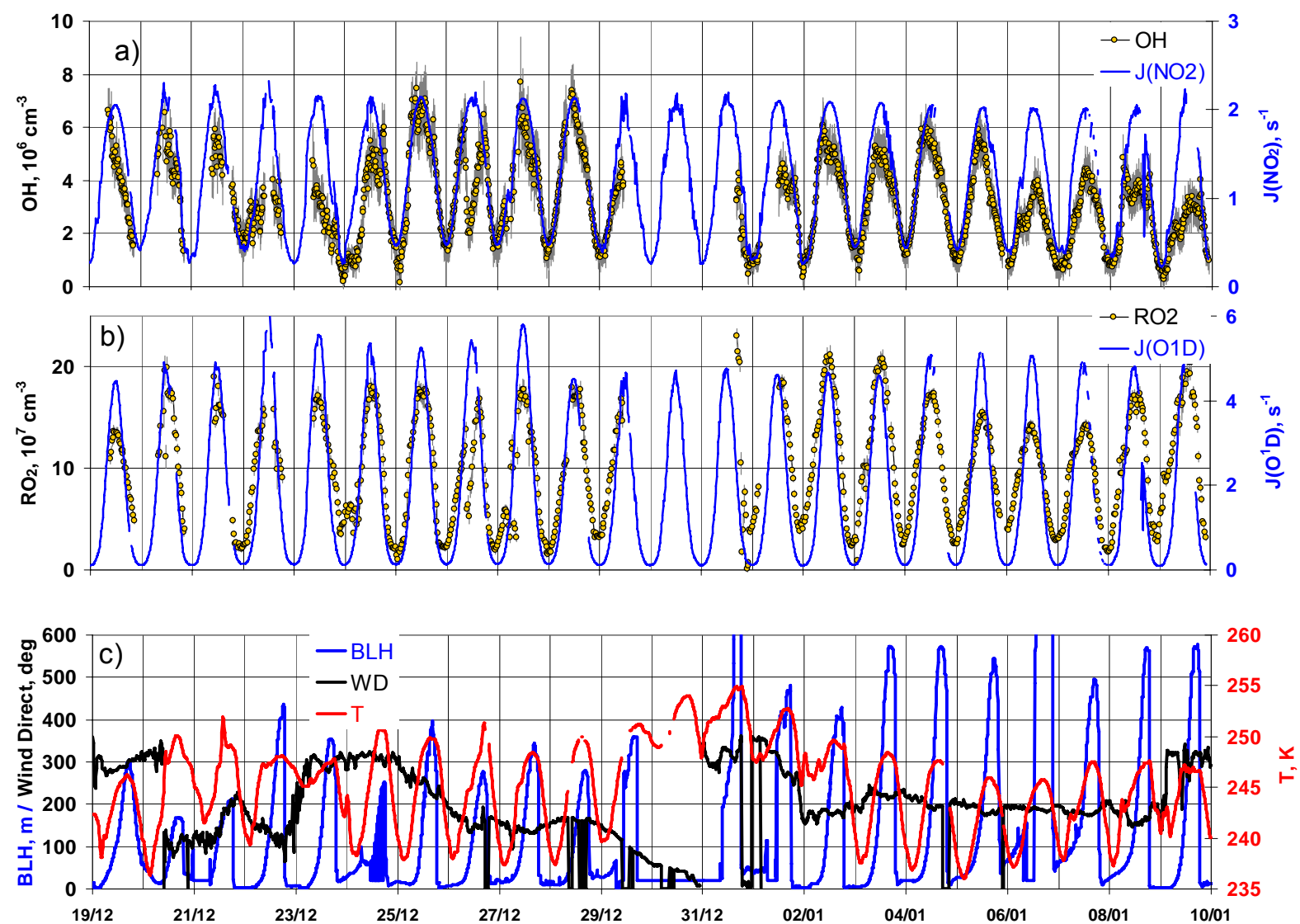b) 1σ uncertainty estimated with accounting for measurement uncertainties

1

2

3

4

5

Figure 1. Temporal profiles at Dome C: [OH], $J(NO_2)$ (a); [RO$_2$], $J(O^1D)$ (b); Wind Direction, temperature and modelled Boundary Layer Height (BLH) (c).

8

9

10

11

12

1

2

3

4

5

6

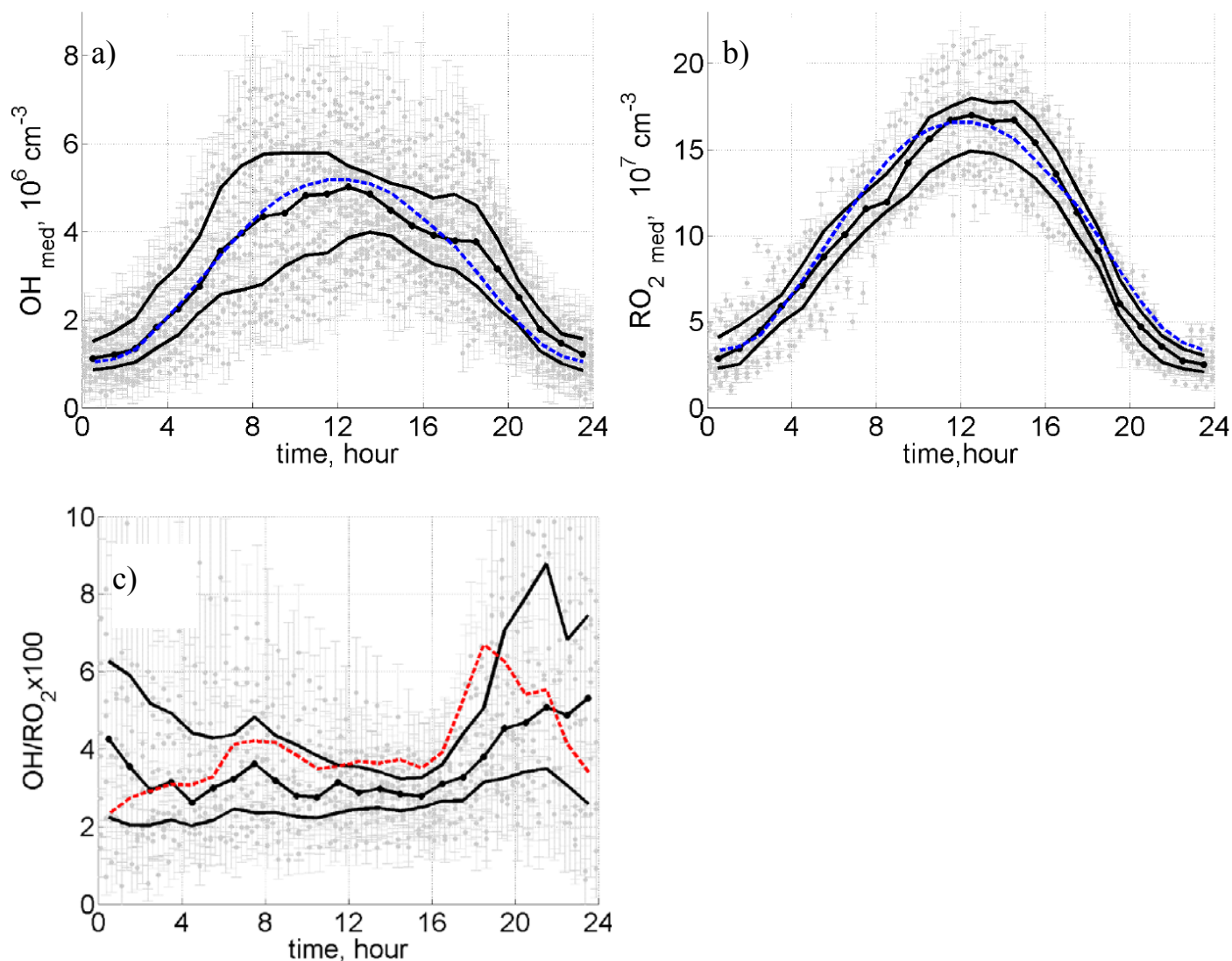**Figure 2**. Median diurnal concentration profiles of OH (a), RO_2 (b), $[OH]/[RO_2]$ ratio (c). Solid lines represent the median and quartile levels. Points – 15 min averaged measured values with standard deviations. Blue line on a) and b) represents $J(NO_2)$ in arbitrary units. Red line on c) represents median NO.

1

2

3

4

5

6

7
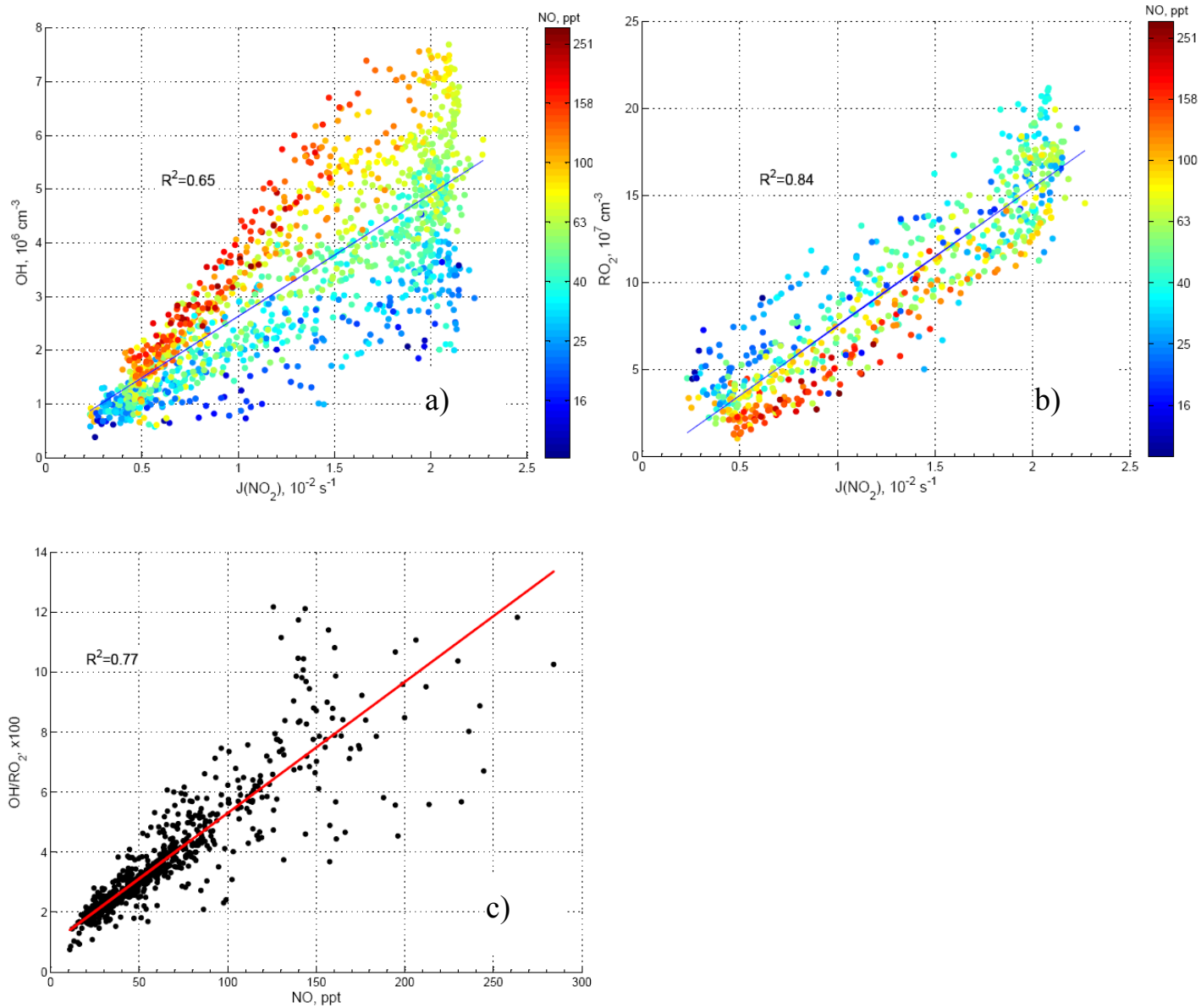
Figure 3. Correlations of [OH] (a) and [RO$_2$] (b) with J(NO$_2$) and of [OH]/[RO$_2$] with [NO] (c).

9

1

2

3

4

5

6
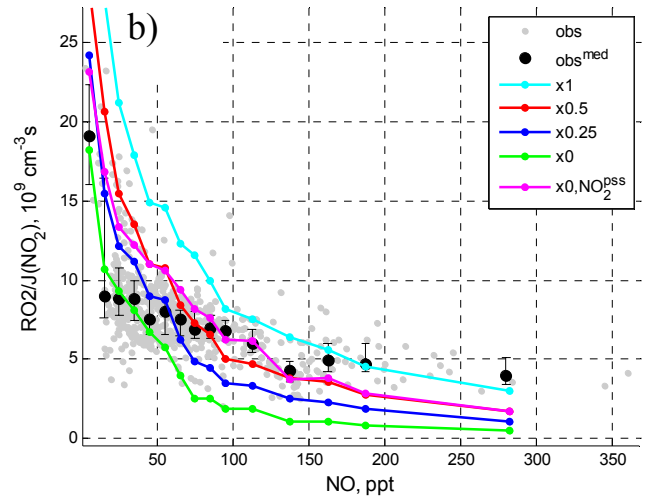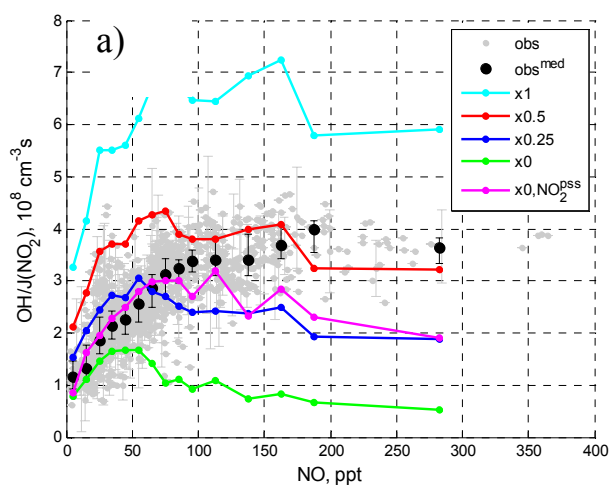
7 **Figure 4**. Normalized concentrations of OH (a) and RO_2 (b) versus measured concentrations of NO. Grey and

8 black points represent observations; colored lines – MCM calculations with [HONO] multiplied by a factor

9 presented in Figure legends (x0 corresponds to estimated steady-state HONO concentrations). Magenta –

10 [HONO]=0 and $[NO_2]$ is calculated by assuming PSS $[NO_2]/[NO]$ ratio.

11
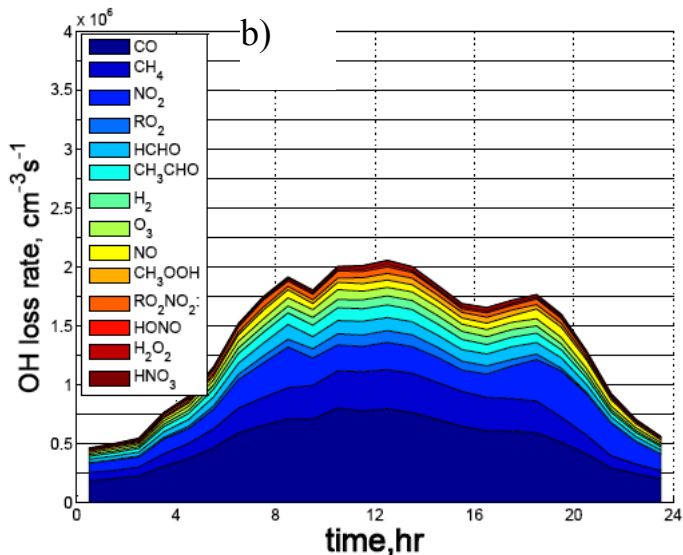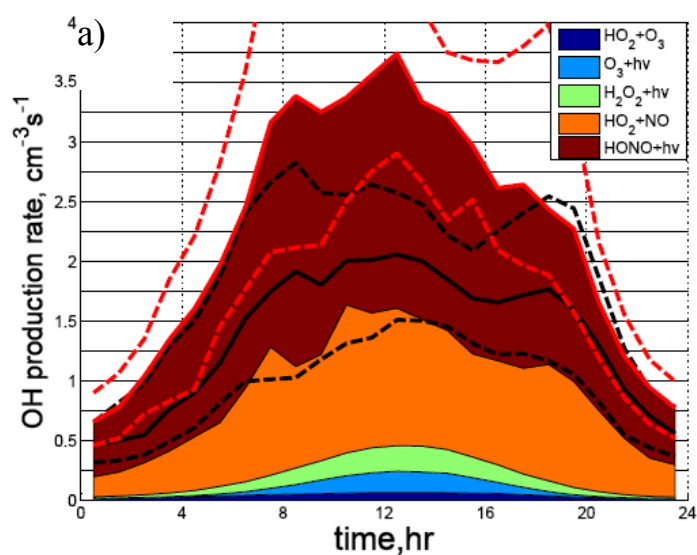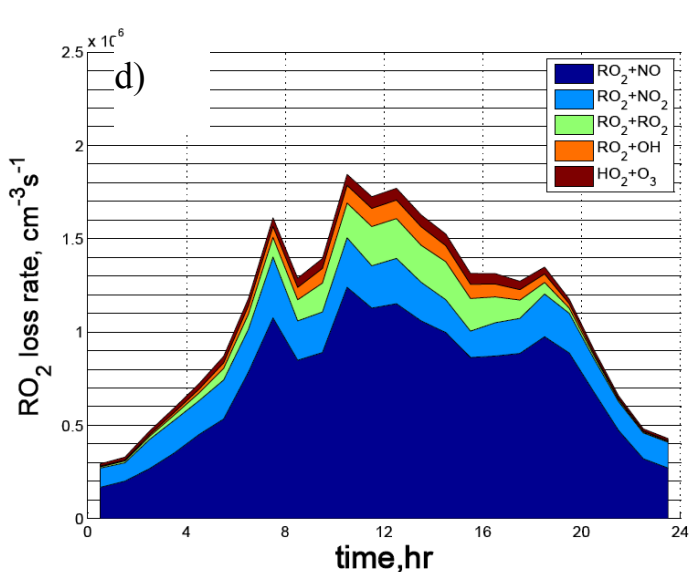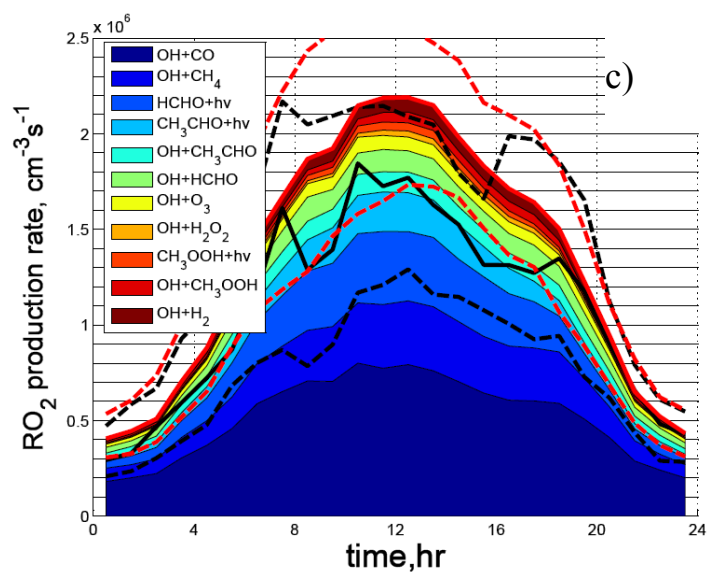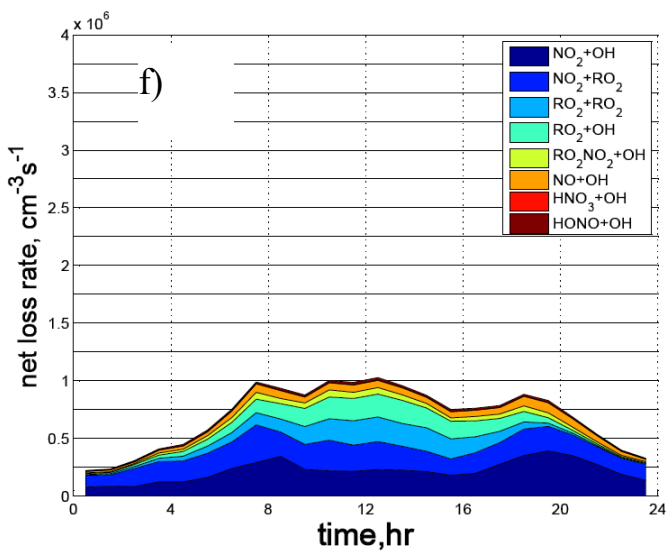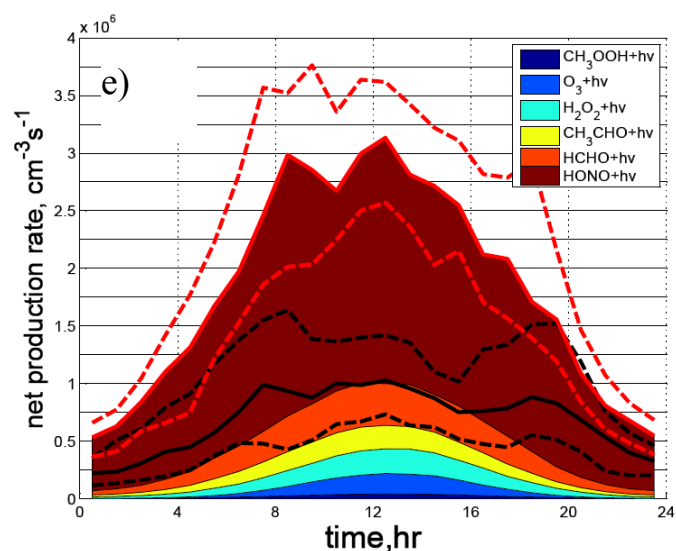
Figure 5. Median diurnal production and loss rates of OH (a,b), RO_2(c,d); net production and loss rates of radicals (e,f). Solid red and black lines represent the total production and loss rates, respectively. Dashed lines correspond to corresponding quartiles.

1

2

3

4

5

6

7
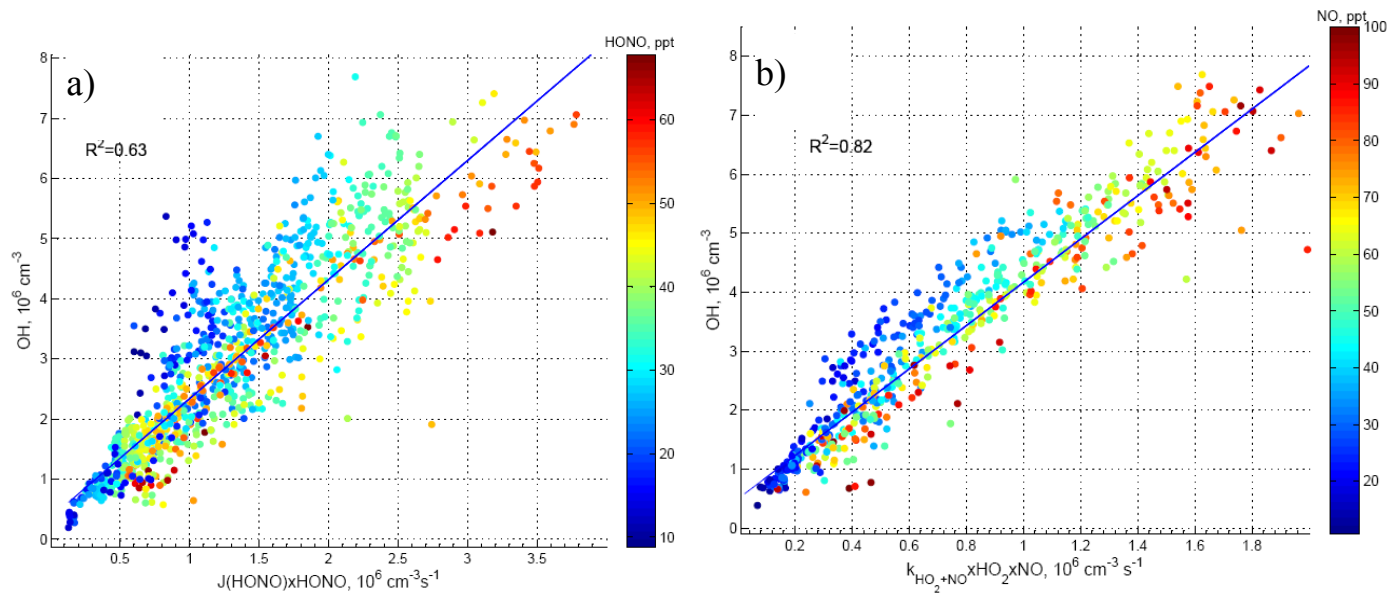
Figure 6. Correlation of measured [OH] with production rates of OH radical by photolysis of HONO, P_{HONO}, (a)
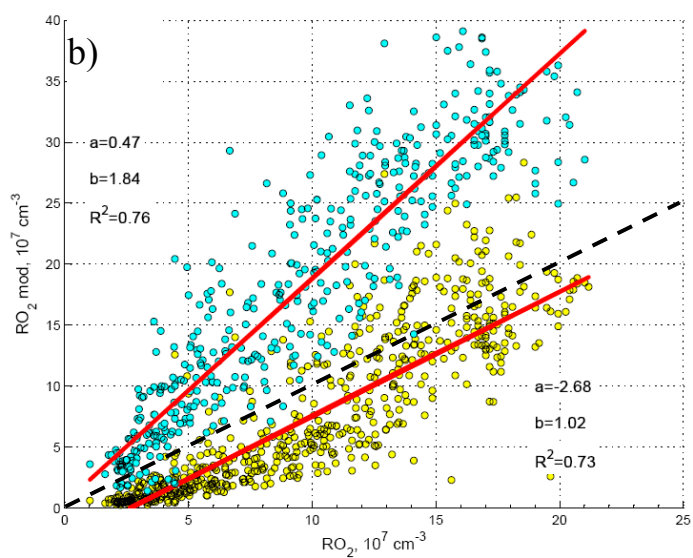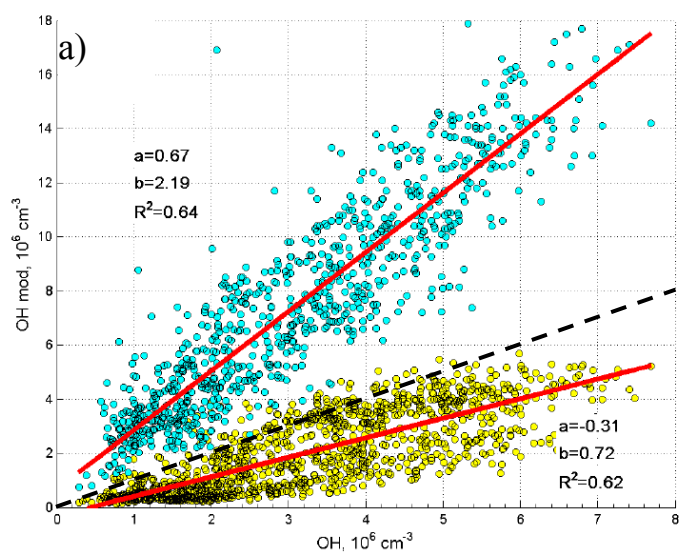
and via reaction HO_2+NO, P_{HO2+NO} (b).

1

2

3

4

5

6

Figure 7. Modelled with the 0-D model vs measured [OH] (a) and [RO$_2$] (b): yellow – with PSS estimated HONO; blue – with measured [HONO]. Coefficients a,b correspond to intercept and slope, respectively. Black lines correspond to linear dependences with a=0 and b=1.
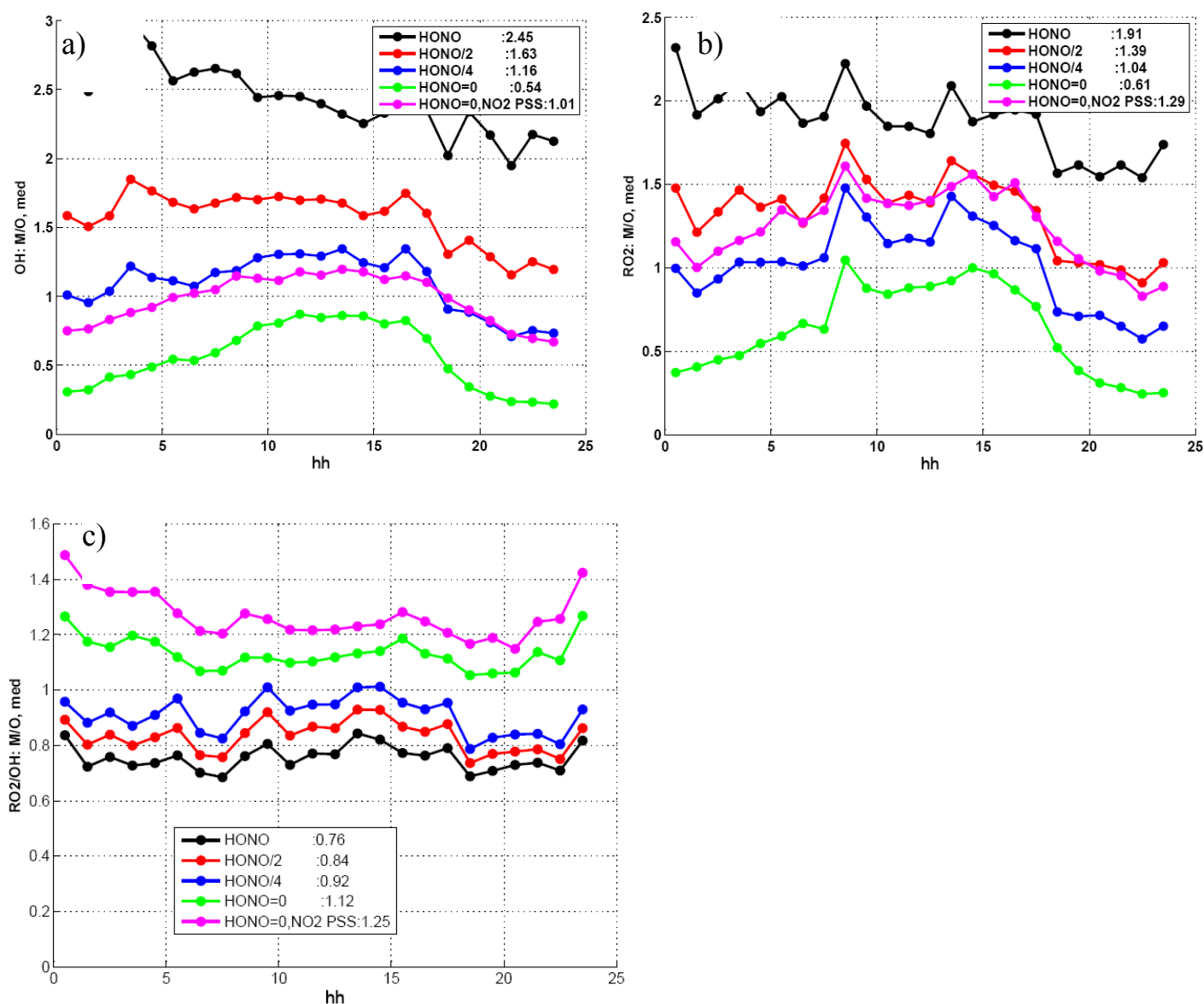
1

2

3

4

5

6 **Figure 8**. Median diurnal Model/Observation ratios for [OH], [RO$_2$] and [RO$_2$]/[OH] at [HONO]=1, 0.5, 0.25, of

7 measured. The "HONO=0, NO$_2$ PSS" curves correspond to the model with [HONO] estimated assuming PSS and

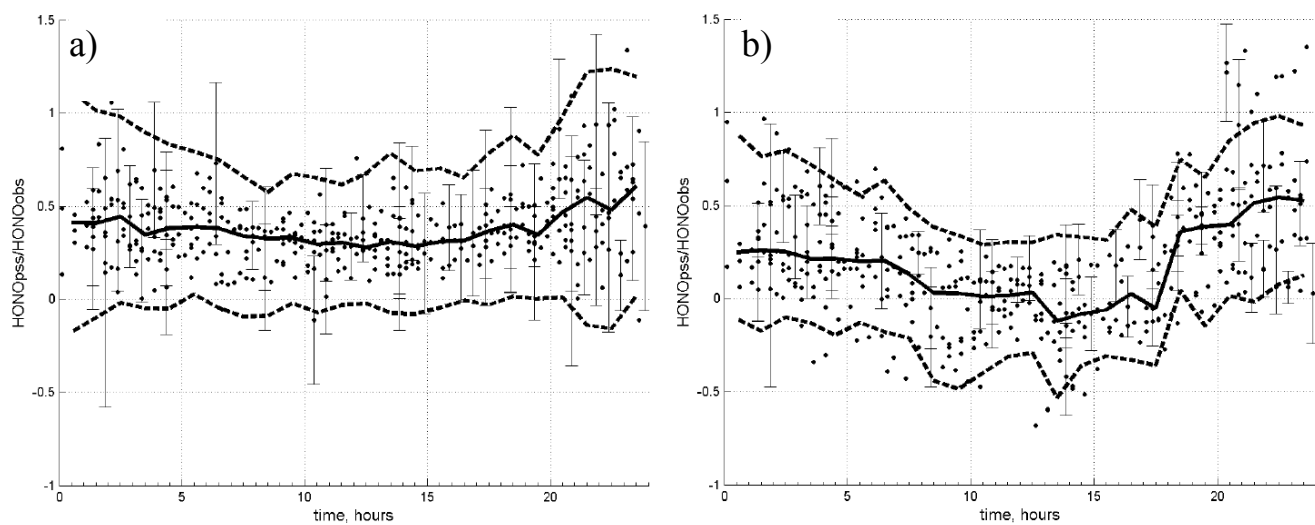8 [NO$_2$] calculated assuming [NO$_x$] at PSS. Numbers in legends represent diurnal median M/O ratios.

9

1

2

3

4

5

6

Figure 9. Ratio of PSS calculated and measured [HONO]: a) from OH budget; b) from net radical (OH and RO_2) sources and sinks. Solid lines – median values; dashed lines- upper and lower quartiles of the mean values with added and subtracted standard deviation, respectively. Error bars correspond to standard deviation.
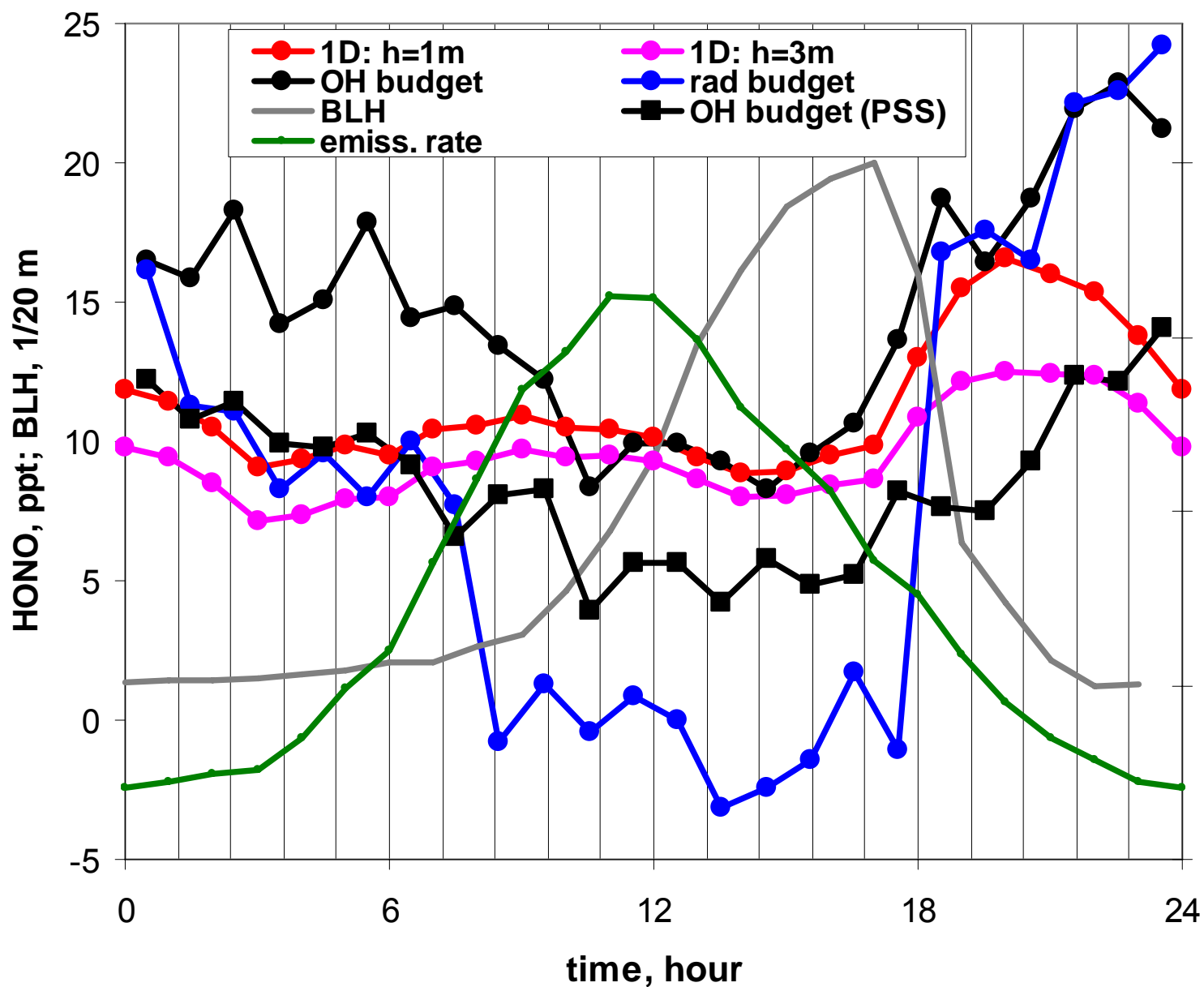
10

1

2

3

4

Figure 10. Comparison of median diurnal profiles of [HONO] derived from OH (black) and sum of radicals (OH and RO_2) (blue) budgets with [HONO] calculated with 1D model at the heights of 1m (red) and 3m (magenta) for the days 2-9 of January. Black circles and squares correspond to [HONO] derived using measured and calculated steady-state [NO_2], respectively. Grey and green lines represent modelled median boundary layer height and HONO emission rates, respectively.
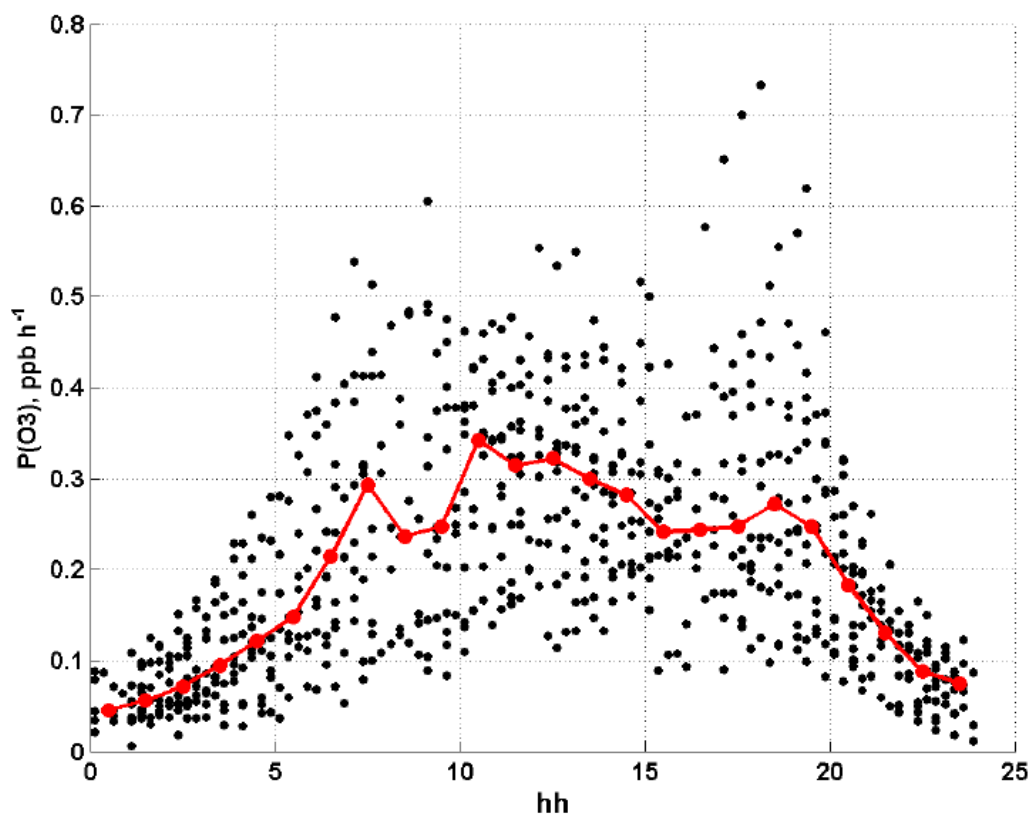
1

2

3

4

5

6

Figure 11. Ozone production calculated from measured [RO$_2$] and [NO]: red line represents hourly median values.

8

9